TÉCNICO LISBOA

Wind Effect in Enhancing PV Performance

Analysis of Wind Speed, Direction, and Convective Heat Transfer on Inclined PV Module at Tennant Creek, Australia

Ziky Teguh Farhan

Thesis to obtain the Master of Science Degree in

Energy Engineering and Management

Supervisors: Prof. Duarte de Mesquita e Sousa
Dr. Jakub Tomczyk

Examination Committee

Chairperson: Prof. Luís Filipe Moreira Mendes
Supervisor: Prof. Duarte de Mesquita e Sousa
Member of the Committee: Dr. Rui Pedro da Costa Neto

December 2021

I declare that this document is an original work of my own authorship and that it fulfils all requirements of the Code of Conduct and Good Practices of the Universidade de Lisboa.

Abstract

Aligning with the Paris agreement to combat climate change, the world is moving towards increasing renewable energy share in the energy mix. The utilization of large scale - Photovoltaic (PV) solar farms has grown significantly throughout the last decade making meteorological data analysis of the area become more crucial than ever in PV solar farm design. PV output is not only decided by solar irradiance but also other important factors such as cell temperature, because high temperature means lower PV efficiency and lifetime. For predicting cell temperature more accurately, analysis of both natural and forced convection are necessary. Studying wind both speed and direction will enrich analytical data for PV yield. Tennant Creek, Australia, is being chosen for this master thesis case location because the area is abundant in solar resources, has plenty of land availability, flat terrain, high ambient temperature and suitable wind data.

This master thesis is presenting PV convection analysis related to solar irradiance, inclination angle, wind speed and wind direction by summarizing from various previous research papers in regard to convection modelling: natural and forced convection. The model factoring frontside and backside of the PV, up-wind or down-wind, flow condition: laminar, turbulent or mixed, and PV characteristic length to determine the convection coefficient. Lastly, calculation of efficiency which results in having higher efficiency of 0.83% compared if wind direction is disregarded and also utility scale PV solar farm design is proposed for case location.

Key words: PV solar farm, Free convection, Wind direction, Forced convection, Convection coefficient, PV convection model.

Resumo

Alinhando-se com o acordo de Paris para combater as mudanças climáticas, a humanidade tem-se posicionado no sentido de aumentar a participação das energias renováveis na matriz energética. A utilização em grande escala de centrais solares fotovoltaicas (FV) cresceu significativamente ao longo da última década, fazendo com que a análise de dados meteorológicos se tornasse mais crucial do que nunca no projeto de centrais solares FV. A produção fotovoltaica depende não só da irradiância solar, mas também da temperatura da célula, com influência direta na eficiência fotovoltaica e vida útil das células FV. Para prever a temperatura da célula com mais precisão, são necessárias análises de convecção natural e forçada. O estudo da velocidade e da direção do vento enriquecerá os dados analíticos para a produção de centrais FV. Tennant Creek, na Austrália, é o local de referência desta dissertação de mestrado porque a área é abundante em recursos solares, pode acolher novas centrais, tem temperatura ambiente bem caracterizada e dados de vento adequados. Esta dissertação de mestrado apresenta uma análise de convecção fotovoltaica correlacionada com a irradiância solar, ângulo de inclinação dos painéis FV, considerando convecção natural e convecção forçada. O modelo analisa o efeito nas faces frontal e posterior dos painéis, e o efeito do vento nas condições de fluxo laminar, turbulento ou misto e, comprimento característico dos painéis FV para determinar o coeficiente de convecção. Por último, o cálculo da eficiência que resulta em ter uma eficiência mais alta de 0,83% em comparação se a direção do vento for desconsiderada e também o projeto de parque solar fotovoltaico em escala de utilidade é proposto para a localização do caso.

Palavras-chave: Central Solar Fotovoltaica, Convecção natural, Direção do vento, Convecção forçada, Coeficiente de convecção, Modelo de convecção fotovoltaico

Acknowledgements

I would like to show gratitude and appreciation to my academic supervisor Prof. Duarte de Mesquita e Sousa and my industrial supervisor Dr. Jakub Tomczyk for their guidance and support during this master thesis journey from start to finish. They provide me with a lot of insight and brilliant ideas as to how I should understand the situation, approach the problem, and how this study can be important in contributing to the future PV model development.

I am very thankful for all the dedication shown by professors, academic supporting staff, fellow students that really helped me in the academic process for the last two years. Also, to Sun Cable Pte. Ltd management for accepting this master thesis proposal and hopefully to be adapted in one of the most ambitious, utility-scale, solar farm projects in the world. Also, my gratitude for the staff for providing necessary data for this research.

Finally, I am very grateful for the love and support from my family and friends. They keep me moving forward.

Table of Contents

List of Figures

List of Tables

List of Symbols

Symbol	Description	Unit
A	PV module area	m^2
g	Gravity acceleration	m/s^2
G	Irradiance	W/m^2
Gr_L	Grashof number	Dimensionless
GTI_{ts}	Corresponding time stamped Global Tilted Irradiance	W/m^2
h	Convection coefficient	W/m^2 K
H	Irradiance incident to PV surface (Faiman)	W/m^2
h_{c_total}	Total free and forced convection coefficient	W/m^2K
h_{free}	Free convection coefficient	W/m^2K
h_{free_bs}	Free convection coefficient back side	W/m^2K
h_{free_fs}	Free convection coefficient front side	W/m^2K
h_{forced}	Forced convection coefficient	W/m^2K
h_{forced_bs}	Forced convection coefficient back side	W/m^2K
h_{forced_fs}	Forced convection coefficient front side	W/m^2K
H_{pv}	PV Height	m
I	Electrical current	A
k	Air Thermal Conductivity	W/m K
L	PV surface length	m
N_u	Nusselt Number	Dimensionless
$\overline{Nu_{L\_fs}}$	Average Nusselt Number	Dimensionless
P_{max}	Maximum electrical power	W
P_r	Prandtl number	Dimensionless
Ra_c	Critical Rayleigh Number	Dimensionless
Ra_L	Rayleigh Number (L)	Dimensionless
Re_L	Reynolds Number	Dimensionless
$Re_{x,c}$	Critical Reynolds number	Dimensionless
S	Perimeter	m

T_{amb}	Ambient temperature	^{o}C or K
T_{pv}	PV temperature	^{o}C or K
T_s	PV surface temperature	^{o}C or K
T_∞	Ambient temperature	^{o}C or K
U'_0	Heat loss coefficient 0	W m^{-2} K^{-1}
U'_1	Heat loss coefficient 1	W m^{-3} K^{-1} s
V_1	Wind speed at PV height (h_1)	m/s
V_{ref}	Wind speed measured at h_{ref}	m/s
v_w	Wind speed	m/s
v_∞	Fluid speed	m/s
W_{pv}	PV Width	m
X_c	Critical length	m
Z_0	Location roughness length	m
β	Fluid volumetric expansion coefficient (only for calculating Rayleigh Number)	/^{o}K
β	PV inclination angle	^{o}
$\beta_{optimum}$	Optimum inclination angle	^{o}
γ	Wind direction	^{o}
μ	Dynamic Viscosity	Kg/ms
ρ	Fluid density	kg/m^3
υ	Air kinematic viscosity	m^2/s

List of Abbreviations

Abbreviation	Description
AM	Air Mass
AOI	Angle of Incidence
CO_2eq	CO_2 Equivalent
DC	Direct Current
DHI	Diffuse Horizontal Irradiance
DNI	Direct Normal Irradiance
EBH	Direct Beam Horizontal Irradiance
gCO_2eq	Gram of CO_2 Equivalent
GHI	Global Horizontal Irradiance
GTI	Global Tilted Irradiance
GW	Giga Watt
HVDC	High Voltage Direct Current
kWh	Kilo Watt Hour
MWh	Mega Watt Hour
LCOE	Levelized Cost of Electricity
MW	Mega Watt
MWp	Mega Watt Peak
NOCT	Normal Operating Cell Temperature
POA	Plane of Arrays
PV	Photovoltaic
STC	Standard Test Condition
USD	US Dollar

1 Introduction

1.1 Motivation

Over the last decade, solar photovoltaic (PV) technology showed significant development in increasing its efficiency and cheaper price. These conditions align with world leaders' commitment to the Paris agreement in increasing their renewable energy shares to their country's energy mix for combating climate change, which made utility scale PV solar farm installation grow rapidly with close to 107 GW addition in 2020 and more than 700 GW total installed capacity globally (IEA, 2021). A utility scale PV solar farm is a solar farm capable of generating more than 1 MW (Seia, 2021). For a solar farm to generate 1 MW a land about 20,000 m^2 is needed. PV cell performance (efficiency and lifetime) is affected by its operating temperature which decreases along with the increase of temperature. Typical PV efficiency is 15% - 20% means that only that much of solar irradiation is converted into electric power while the rest is converted into heat. 1% increases or decreases in efficiency can be considered significant for above 1 MW solar farms. Thus, predicting PV temperature becomes more important than ever.

Many PV solar farms are being built either on barren lands, mountains, desert or any flat terrain with plenty of wind as heat transfer medium for cooling down PV surfaces. Optimizing wind speed and direction for reducing heat on a PV module can be important factors to increase PV performance. Although the study of natural convection from plate with arbitrary inclination angle is dated back to 1972 (Fujii & Imura, 1972) and forced convection 1977 (Sparrow, 1977), current widely used “bankable” modelling softwares (PVSyst and Helioscope) only accommodate wind speed but not wind direction in their model. The purpose of this research is to propose a utility scale solar farm design factoring natural wind flow to improve PV performance through convective heat transfer. The impact of wind flow parameters such as wind velocity, temperature, direction, turbulence on PV module structure and tilt angle and orientation will be analyzed to model the solar farm output. An experiment for the similar topic has been conducted (Glick & Ali, 2020) but not yet implemented in a model where optimum output solution can be derived.

Tennant Creek, Australia, is chosen as a case study because it has plenty of land availability, flat terrain, high ambient temperature and suitable wind data makes the location a good site for this research. Even though Australia has good solar irradiation, Figure 1, since the solar farm will be in a flat terrain barren area with low roughness length, means that while it has lower wind obstruction but also has high ambient temperature that will increase the PV cell operating temperature. Developing the model, the author collaborated with Sun Cable Pte Ltd which planned to construct a 13 GW solar farm in Australia to provide 20% of Singapore Electricity, which mostly comes from natural gas, via HVDC (High Voltage Direct Current) submarine cable which will provide adequate information regarding solar irradiance and wind parameters data.

1.2 Research hypothesis and goals

Utility-scale PV solar farms require large capex or investment, this is the reason why PV energy yield analysis for the solar farm location becomes most important. Since popular PV models only factor wind speed, a study for wind direction is needed to give a better approach determining PV performance. Thus, the research goals of this master thesis are:

- Analyze location's meteorological data that will be used for modelling such as: solar irradiance, solar zenith and azimuth angle, ambient temperature, and wind characteristics (speed and direction).
- Summarizing equations being used for the model in the simplest way.
- Developing a model to correlate between PV technical specification, inclination angle, wind speed and direction, flow characteristic for front and back PV surface, and convection coefficient to PV performance.

1.3 Scope and limitation

This master thesis scope is limited only to analyze convection heat transfer on ground fixed north/south faced PV solar farms. The study will be performed only by simulation using software, which is Microsoft Excel and Helioscope. The location chosen for the analysis is solely on Tennant Creek, Australia, with its specific meteorological profile.

When evaluating the results, the thesis is focused on convection coefficients for predicting PV performance. Since there are many convection models from different research journals regarding natural convection and forced convection, this thesis tries to accommodate the most relevant with the location condition. Conductive heat transfer is neglected in this thesis since PV temperature for both front and backside is considered the same, while in reality the difference could be from 0 – 3^{o}C. Radiative heat transfer and data analysis from on-site testing is also not included in this study and will be important for future work to further develop the model.

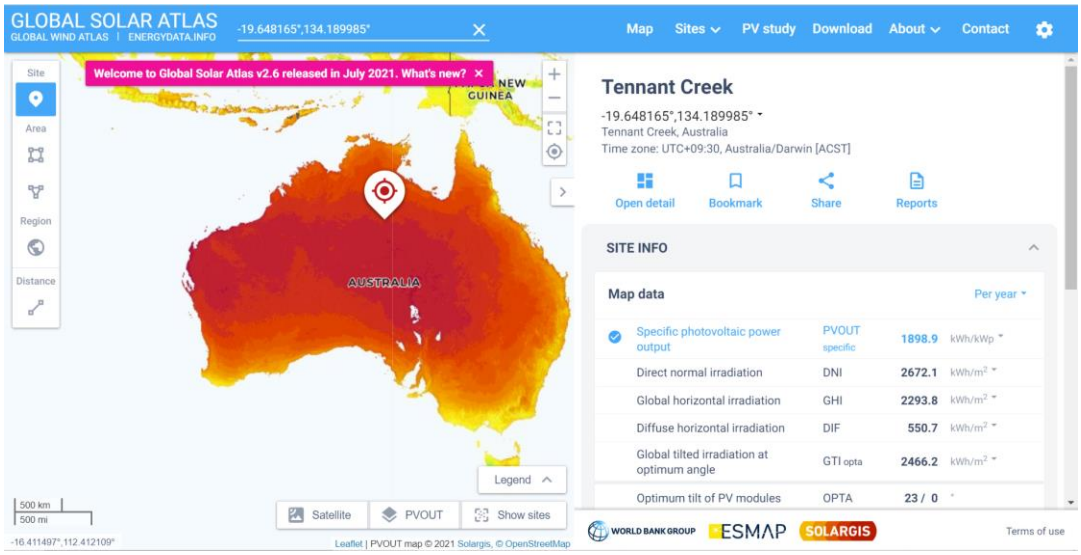

Figure 1Tennant Creek, Australia adapted from globalsolaratlas.info

1.4 Thesis structure

This master thesis structured as follows:

- Chapter 2 provides literature review for models and equations that are being used along with other important information.
- Chapter 3 presents methodology to formulate the PV model including site analysis, flowchart for model calculation and other parameters
- Chapter 4 discusses the model and calculation result from meteorological data such as: solar irradiance, wind parameter, inclination angle against PV convection coefficient.
- Chapter 5 contains the conclusion of the research and suggestions for future works that can be done for improving the model.

2 Literature Review

2.1 Photovoltaic temperature effect

Standard test (STC) for measuring PV I-V characteristic is inside a lab with irradiance of 1000 W/m^2, air mass 1.5 spectrum (AM 1.5) and cell temperature of 25^o C. PV power output is a combination of its voltage and current. Current is more affected by solar Irradiance with almost linear relation $G_1/G_2 \approx I_2/I_1$ Where G_1 & G_2 are different value of Irradiance (W/m^2) and I_1 & I_2 are the corresponding electrical currents (A). PV voltage output is highly determined by the cell operating temperature. The nominal operating cell temperature (NOCT) for PV is measured by open circuiting the cell under Irradiance of 800 W/m2, air temperature of 20^o C and 1 m/s wind velocity. For the same irradiance PV output can vary depending on its operating temperature. The PV I-V curve in the Figure 2 shows the change of the curve when cell temperature increases while receiving the same solar irradiance.

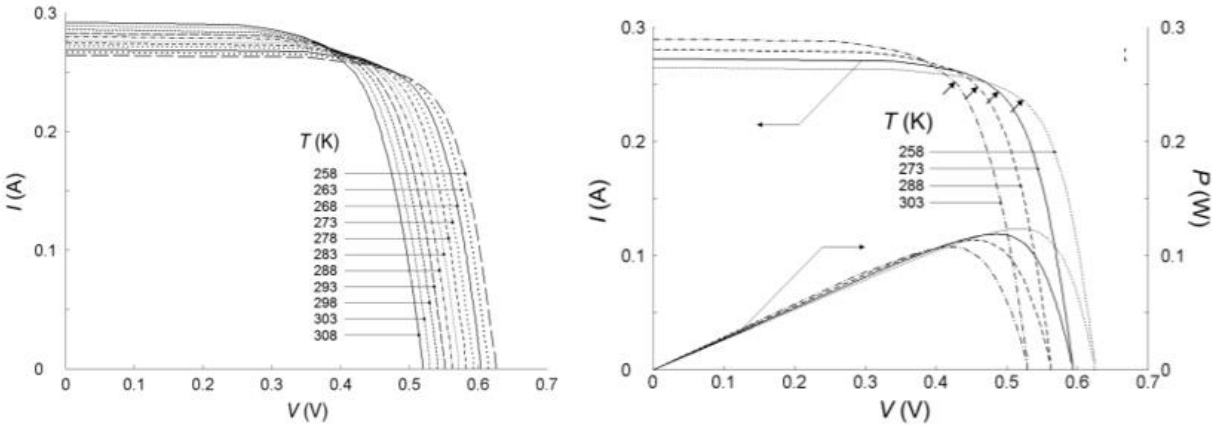

Figure 2 Typical PV I-V curve for different operating temperature adapted from (Libra & Poulek, 2017)

From the graph on the right side of Figure 2 we can see that the higher the temperature resulting in a smaller maximum power output. The curve depends on PV material and manufacturers usually provide technical specifications related to decreasing efficiency when PV operates at a higher temperature than its NOCT.

2.2 Faiman model

In reality, PV modules often operate more than its rated NOCT especially in locations where ambient temperature is high and from experiments higher irradiance translates to higher PV temperature. Since predicting PV temperature becomes the first task for predicting PV output accurately, a model which correlates PV temperature, ambient temperature, plane of array irradiance (POA) is being proposed by Faiman (Faiman, 2008).

$$T_{pv} = T_{amb} + \frac{H}{U'_0 + U'_1 \times v_w} \quad \text{(Eq. 1)}$$

Where T_{pv} and T_{amb} are PV and ambient temperature, *H* is total irradiance incident to PV surface during measurement, *U'₀* and *U'₁* are constants, and the value can vary between PV type and manufacturer from experiments. Even though in the Faiman paper the equation is written $T_{mod} = T_{mod} + H/(U'_0 + U'_1 \times v_w)$ in eq (5) the rest of the paper calculation is aligned with (Eq.1) of this thesis. Offering a simple equation, most PV softwares currently only uses the Faiman model for predicting PV temperature which doesn't take into account wind direction. But this simplicity has a drawback that is the model potentially under-estimating energy yield for solar farms with high wind velocity from the backside of PV module and over-estimating the one with low wind velocity from front-side of PV module. This will be discussed in further chapters.

Table 1 Thermal constant for different module type from (Faiman, 2008)

Module type	U'_0 (W m^{-2} K^{-1})	U'_1 (W m^{-3} s K^{-1})	RMS error (°C)
Solarwatt MHH plus 170	24·1	7·12	2·13
Solar-Fabrik SF 150/2-142	24·0	7·68	2·12
Solar World SW200 poly	25·7	7·25	1·88
RWE Schott Solar ASE-165-GT-FT/MC	23·5	7·66	1·96
Shell Solar Power Max Plus 165-C	25·7	6·68	1·93
Scheuten Multisol 180 P6	26·4	6·25	1·85
Solon P220/6+	24·9	6·33	1·99
Combined Fit	25·0	6·84	1·86

PV thermal constants being used in this thesis are U'_0 = 25 W m^{-2} K^{-1} and U'_0 = 1.2 W m^{-3} s K^{-1}. The temperature coefficient to maximum power from the manufacturer is P_{max}=-0.35%/°C meaning PV output power decreases 0.35% every 1°C increase.

2.3 Experiment with wind direction

Although wind speed is a very important factor, but experiment conducted by (Glick & Ali, 2020) in Figure 3 stating that wind direction, PV inclination angle and PV arrangement can determine PV solar farm output. They studied the fluid flow that drives heat transfer and determined how much temperature can be reduced by improving the convection of the array. The experiment results showed a possible 30-45% significant increase in convective heat transfer coefficient, depending on the incoming wind direction and PV module inclination angle, leading to potential power efficiency increase of ~5% and solar panel degradation decrease of +0,2%

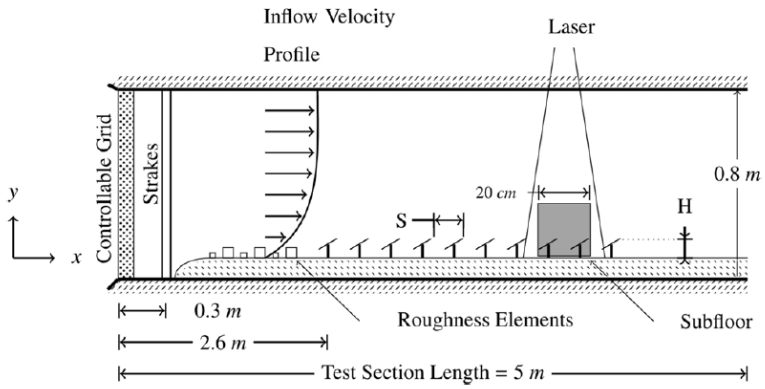

Figure 3 Wind tunnel experimental set up (Glick & Ali, 2020)

The experiment was conducted in a wind tunnel experimental setup with 40 individual panels arranged into 10 rows. The solar array experimental platform was designed to scale properly to utility scale. The convergence tests were taken to ensure the experimental platform has enough row spacing and flow convergence. The tests showed that the flow after 6-7 rows were fully developed, so the data taken between row 8-9. The results in Figure 4 and Figure 5 shows the highest turbulence flow happened when the wind flowing from the back of PV (h).

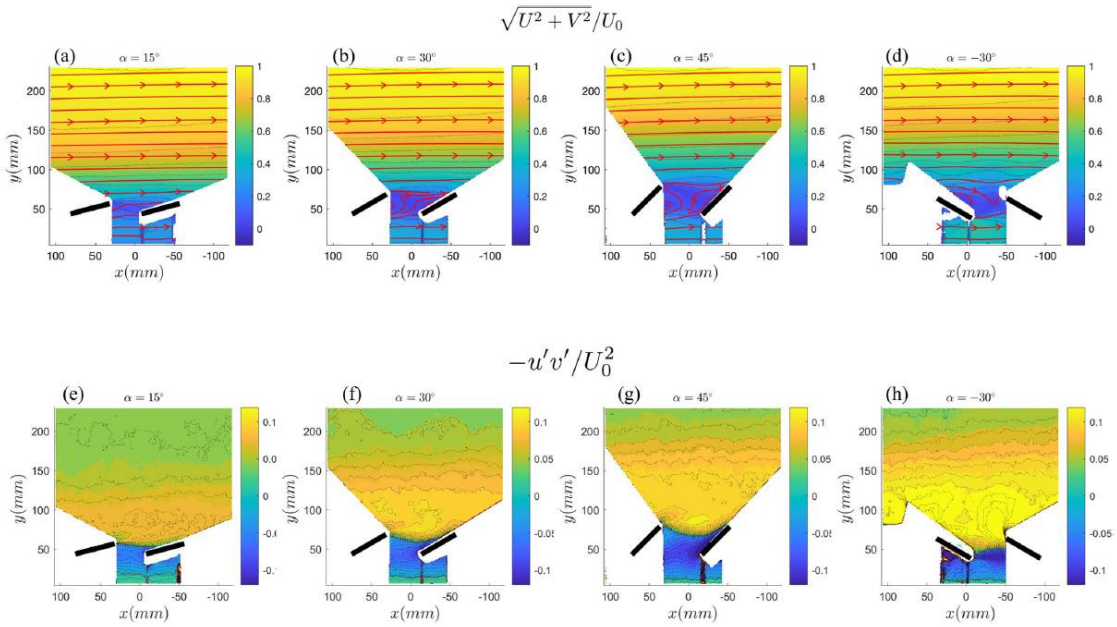

Figure 4 Normalized mean velocity and Reynolds shear stress profiles (Glick & Ali, 2020)

Two basic parameters used in this experiment were wind speed and inclination angle. PV inclination angle was chosen [15°, 30°, 45°, −30°] to represent arrangements of different latitudes. Negative inclination angles represent the same standard solar farm with a tilt of 30°, where the wind flows from the back side

of the PV because the wind source is only one and the flow is from left to right. Figure above shows the flow field in normalized, ensemble-averaged velocity magnitude spatial contours and Reynolds shear stress across four inclination angles plotted in particle image velocimetry (PIV) spatial window.

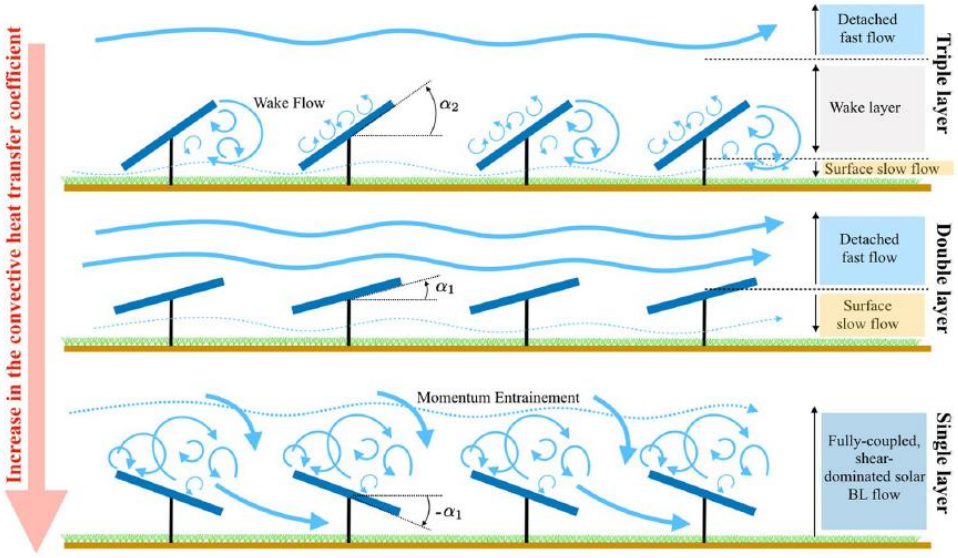

Figure 5 Inclination angle and convective heat transfer (Glick & Ali, 2020)

Experiments with tilt angles of -30^0 and +30^0 indicated the significant difference of heat transfer coefficient by 30% to 45%. The more wind flowing from the back side of PV the more turbulent the flow on front side as in Figure 5. This study suggested the PV array to be designed to take advantage of passive convective cooling. If the incoming flow faces the rear surface or upwind backside of the PV panels, the significant increase in heat transfer coefficient occurred. This leads to a 5-9^0 C decrease in PV module temperature and potential power efficiency of ~5% and reduction of panel degradation. The wind direction in this experiment is only for two different angles, upwind frontside (0 degree) and upwind backside (180 degree). Even though there is no model for convection that is being proposed from the experiment, it shows an important result that wind direction can play a major role for increasing PV performance.

2.4 Convection model

To factor wind speed and wind direction in determining PV temperature, convective heat transfer between the fluid flowing (air and wind) with both frontside and backside of PV surface is being analyzed. In convective heat transfer, it is well known that Newton general expression for cooling can be referred $Q = h \cdot (T_s - T_\infty)$ Where h is convection coefficient, T_∞ and T_s are ambient and surface temperature. While the convection model is not something being done only recently, many PV software developers pay little attention to it because the theoretical equation usually based on specific conditions and accommodating them for general use became more of a complex work since the Faiman model already provides a good prediction. But if we consider a utility-scale solar PV farm the energy yield difference between models can

be noticeable. Previous study and modelling were developed based on similar cases such as convection on inclined plate, solar collector, and even solar PV module. There are two types of convection happening on PV modules in open space solar farms: natural or free convection and forced convection.

2.4.1 Natural / free convection

Free convection happens when a different temperature of a surface interacts with fluid under gravity and in the absence of external force. The temperature difference between PV surfaces and surrounding fluid (air) causes the density to change resulting in the buoyancy force will start to take effect. This phenomenon makes the previously stagnant fluid begin to move and carry the heat. One important constant in convection heat transfer is Nusselt number (N_u) which relates convection coefficient with fluid thermal conductivity (k) and surface characteristic length (L) in this general expression $N_u \equiv h \cdot L/k$. Flows of natural convection vary in accordance with the surface inclination angle and temperature (Fujii & Imura, 1972) since PV have front and back surfaces the flow behavior can be different. Thus, the Nusselt number for both sides need to be determined. Rayleigh number is calculated for predicting the fluid flow characteristics, whether it's laminar or turbulent. The Rayleigh number for an inclined plate is expressed with the equation 2 (Eq. 2) (Tuncel & Akinoglu, 2018).

$$Ra_L = \frac{g \cdot \beta \cdot \left(T_{pv} - T_{amb}\right) \cdot cos\theta \cdot L^3}{\alpha \cdot v} \quad \text{(Eq. 2)}$$

Where g is gravity acceleration β is fluid volumetric expansion coefficient or $2/(T_{pv} + T_{amb})$ and the temperature unit is in Kelvin. Although in the paper β is written as $1/(T_{pv} + T_{amb})$ in eq. 4. but other reference papers are supporting this thesis of (Eq.2) (Bergman, 2011). θ is 90 – PV inclination angle in degree and L is the characteristic length of natural convection air flow in contact with the PV module, α is air thermal diffusivity and v is air kinematic viscosity. If the calculated Rayleigh number is higher than the critical Rayleigh number, the flow is considered turbulent and if lower the flow is laminar. For most cases, where the shape of the flow boundary layer is similar with natural convection on vertical plate which is showing a smooth shape of boundary layer, critical Rayleigh number is 10^9 but for a flow in certain condition such as on the frontside of high temperature PV which the flow tends to be turbulent, critical Rayleigh number is $Ra_c = 10^{8.9-0.00178*\theta^{1.82}}$) (Mittag & Vogt, 2019). Related to free convection, there are two modes of PV operation: cold plate and hot plate. Hot plate mode is considered when PV surfaces temperature are higher than ambient temperature, which is mostly the case when PV is in a steady operation generating electricity. Cold plate mode is when PV surfaces are colder than ambient temperature while generating electricity. This situation can happen when solar irradiance is still low.

When PV operates as a hot plate, the buoyancy flow on the frontside and backside can be referred to in the Figure 6 from (Bergman, 2011) and (Fujii & Imura, 1972) experiment.

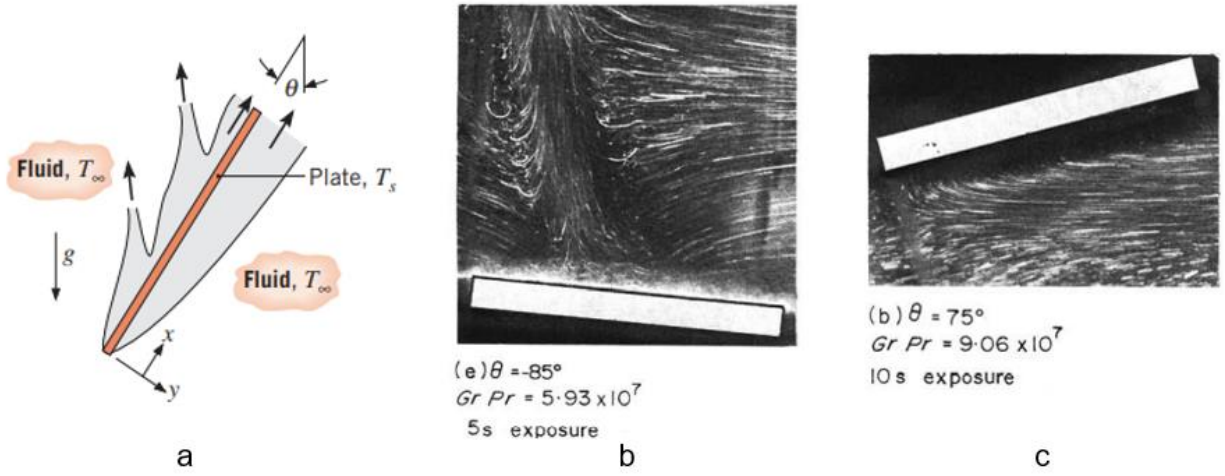

Figure 6 Flow pattern of PV surfaces operating as hot plate (Bergman, 2011) & (Fujii & Imura, 1972)

Figure 6 (a) and (b) showing the flow pattern for the PV frontside since flow tends to separate midway and the shape of the boundary layer is not smooth. In this condition the critical Rayleigh number equation from (Mittag & Vogt, 2019) is being used. From (a) and (c) it is shown that the flow on the backside of PV shows a similar pattern to the vertical plate, thus we can use 10^9 as the Rayleigh critical number for $0 \leq \theta < 60°$. Since β or PV inclination angle to the horizon is more popular term, $\theta = 90 - \beta$. Average Nusselt number of PV sides for different conditions are in correlation with Rayleigh number and θ. This can be seen in the Table 2 & Table 3.

Table 2 Free convection equations for PV frontside operates as a hot plate

Frontside	Average Nusselt Number $\overline{(Nu_{L\_fs})}$	Reference	Eq.
$Ra_L \leq Ra_C$	$0.56\ {Ra_L}^{1/4}$	(Fujii & Imura, 1972)	3
$Ra_L > Ra_C$ & $\theta \geq 60°$	$0.13\ {Ra_L}^{1/3}$	(Fujii & Imura, 1972)	4
$Ra_L > Ra_C$ & $\theta < 60°$	$0.13 \cdot \left[\left(\frac{Ra_L}{cos\theta}\right)^{1/3} - {Ra_C}^{1/3}\right] + 0.56 \cdot (Ra_C \cdot cos\theta)^{1/4}$	(Fujii & Imura, 1972)	5

For PV frontside operates as a hot plate, If the Rayleigh number for a surface *L* (Ra_L) is smaller than the calculated Rayleigh critical number (Ra_c) the flow is laminar, hence the average Nusselt number ($\overline{Nu_{L\_fs}}$) is calculated by Eq.3. If Ra_L is higher than Ra_c the flow is considered turbulent. Another checking parameter for turbulent flow is the θ. For θ close to horizontal ($\geq 60^o$) Eq.4 can be used and for θ angle less than 60^o the average Nusselt number can be calculated by using Equation 5 (Eq. 5).

Table 3 Free convection equations for PV backside operates as a hot plate

Backside	Average Nusselt Number $\overline{(Nu_{L\_bs})}$	Reference	Eq.
$Ra_L \leq 10^9$ & $0 \leq \theta < 60°$	$0.68 + \frac{0.670 {Ra_L}^{1/4}}{[1+(0.492/Pr)^{9/16}]^{4/9}}$	(Bergman, 2011)	6.a
$Ra_L > 10^9$ & $0 \leq \theta < 60°$	$\left\{0.825 + \frac{0.387 {Ra_L}^{1/6}}{[1+(0.492/Pr)^{9/16}]^{8/27}}\right\}^2$	(Bergman, 2011)	6.b
$10^5 \leq Ra_L \leq 10^{11}$ & $60° \leq \theta < 88°$	$0.56\ {Ra_L}^{1/4}$	(Fujii & Imura, 1972)	7
$10^6 \leq \frac{Ra_L}{cos\theta} \leq 10^{11}$ & $88° \leq \theta < 90°$	$0.56 \left(\frac{Ra_L}{cos\theta}\right)^{1/5}$	(Fujii & Imura, 1972)	8

When PV backside operates as a hot plate, for $0 \leq \theta < 60°$, the boundary layer shape is like that of a vertical plate thus, the Rayleigh critical number of 10^9 can be used. If calculated $Ra_L > 10^9$ the flow is turbulent and average Nusselt number ($\overline{Nu_{L\_bs}}$) calculation is based on Eq. 6.a. If $Ra_L \leq 10^9$ the flow is laminar and $\overline{Nu_{L\_bs}}$ calculated by Eq 6.b where *Pr* is Prandtl number, and the value can be consulted in the air properties table. For most sites near the earth equator the optimum PV tilt angle is up to 30° or ($60° \leq \theta < 88°$) thus, the Nusselt number is calculated by Eq.7. For an almost horizontal plate, $\overline{Nu_{L\_bs}}$ is estimated by Eq. 8.

During cold plate mode operation, the opposite happens. The frontside has a smoother flow layer while the backside tends to be more turbulent and the flow travels from top to bottom as can be seen in the Figure 7.

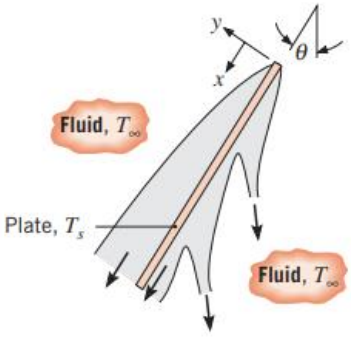

Figure 7 Flow pattern of PV surfaces operating as cold plate adapted from (Bergman, 2011)

The behavior of air flow in natural convection when PV operates as a cold plate is the opposite to that of hot plate. The leading edge is the top of PV height and trailing edge is the bottom. PV frontside boundary layer shape has more regular transition from laminar to turbulent compared to the backside. Thus, the

average Nusselt number equation for frontside hot plate can be used to backside the cold plate and vice versa. Following table is equation for cold plate state

Table 4 Free convection equations for PV operates as a cold plate

Frontside	Average Nusselt Number $\overline{(Nu_{L\_fs})}$	Eq
$Ra_L \leq 10^9$ & $0 \leq \theta < 60°$	$0.68 + \frac{0.670 {Ra_L}^{1/4}}{[1 + (0.492/Pr)^{9/16}]^{4/9}}$	6.a
$Ra_L > 10^9$ & $0 \leq \theta < 60°$	$\left\{0.825 + \frac{0.387 {Ra_L}^{1/6}}{[1 + (0.492/Pr)^{9/16}]^{8/27}}\right\}^2$	6.b
$10^5 \leq Ra_L \leq 10^{11}$ & $60° \leq \theta < 88°$	$0.56\ {Ra_L}^{1/4}$	7
$10^6 \leq \frac{Ra_L}{cos\theta} \leq 10^{11}$ & $88° \leq \theta < 90°$	$0.56\ \left(\frac{Ra_L}{cos\theta}\right)^{1/5}$	8
Backside	Average Nusselt Number $\overline{(Nu_{L\_bs})}$	Eq
$Ra_L \leq Ra_C$	$0.56\ {Ra_L}^{1/4}$	3
$Ra_L > Ra_C$ & $\theta \geq 60°$	$0.13\ {Ra_L}^{1/3}$	4
$Ra_L > Ra_C$ & $\theta < 60°$	$0.13 \cdot \left[\left(\frac{Ra_L}{cos\theta}\right)^{1/3} - {Ra_C}^{1/3}\right] + 0.56 \cdot (Ra_C \cdot cos\theta)^{1/4}$	5

From the above equation, the Nusselt number is higher when the flow is turbulent for both frontside and backside of the PV. Higher Nusselt means higher natural convection coefficient (*h*) since the fluid carrying the heat will move and be replaced faster. As the θ angle is closer to 90°, meaning close to horizontal, PV backside becomes more insulated and behaves similar to a solar collector which is common to be installed with one side thermally insulated. PV inclination angle from horizontal (*β*) in this thesis is not considered to be installed horizontally with zero slope. This is in consideration of that for rainwater and dirt to fall thus minimizing soiling. To maintain the PV 'self-clean' some degree of inclination needs to be adapted and, in this Thesis, the minimum *β* is above 2°.

2.4.2 Forced convection

Forced convection happens when there is an external force driving the fluid flow, for PV case is the wind. Refer to (Glick & Ali, 2020) experiment for forced convection wind direction and PV module orientation can be a factor to determine flow characteristics for both PV sides because they are affecting one another. Similar with free convection, one important constant in forced convection is Reynolds number as fluid's ratio of the inertia and viscous force (Bergman, 2011).

$$Re_L = \frac{\rho \cdot v_\infty \cdot L}{\mu} \quad \text{(Eq. 9)}$$

Where ρ, v_∞, and μ are fluid density, velocity, and viscosity. L is the characteristic length of the surface that is in contact with the fluid flow. For upwind surface characteristic length represents the distance between from leading edge to trailing edge. If we consider γ as the angle difference between PV azimuth and wind direction where 0º represents North and act as reference, characteristic length for PV surfaces when upwind and $|\gamma| \leq 45°$ is the PV height and when $|\gamma| > 45°$ the characteristic length is the PV width. Relation between PV Azimuth, wind direction, and inclination angle are in Figure 8.

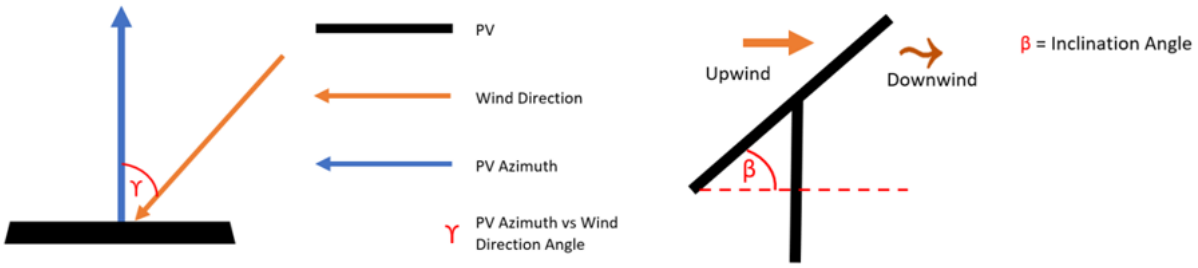

Figure 8 PV Azimuth vs Wind direction

For downwind PV surface since wind speed and orientation is not relevant the characteristic length is $L = 4 \cdot A/S$ where A is PV module area and S is its perimeter (Kaplani & Kaplanis, 2014). The relation between γ and L is in the following table.

Table 5 Forced convection characteristic length

ϒ (degree)	Frontside	Backside
$0 \leq \gamma \leq 45$ Or $315 \leq \gamma \leq 360$	L = PV Height	$L = 4 \cdot A/S$
$45 < \gamma \leq 90$ Or $270 \leq \gamma < 315$	L = PV Width	$L = 4 \cdot A/S$

$90 < \gamma < 135$ Or $225 < \gamma < 270$	$L = 4 \cdot A/S$	L = PV Width
$135 \leq \gamma \leq 225$	$L = 4 \cdot A/S$	L = PV Height

Synonymous with Rayleigh number to determine flow condition in natural convection, Reynolds number is used to determine the flow condition in forced convection. By using the ratio between critical length and characteristic length the condition can be predicted whether it's a laminar, turbulent, or mixed. Rearranging Eq. 9 we can have $x_c = Re_{x,c} \cdot \upsilon / v_w$ where x_c is critical length, $Re_{x,c}$ is critical Reynolds number or 4 x 10^5, $\upsilon \; and \; v_w$ are air kinematic viscosity and speed. From (Sartori, 2006) if $x_c \ll L$ it is considered the flow is fully turbulent and if $x_c \geq 0.95\, L$ indicating that the flow is laminar and if $x_c < 0.95\, L$ the flow is in transition from laminar to turbulence or a mixed flow condition.

Another equation to estimate forced convection is proposed by (Kendoush, 2009) by accommodating wind speed and direction incidence to the PV surface. Based on (Kaplani & Kaplanis, 2014) experiment, (Kendoush, 2009) general equation provides more accurate result for upwind PV surface and (Sartori, 2006) is being used for downwind and backside PV surface. Figure 9 explained that the wind incidence angle (α_w) is calculated from $\alpha_w = cos\,(\gamma) * \cos\,(90 - \beta)$

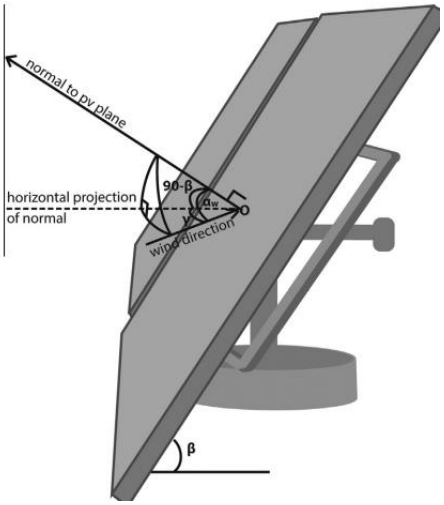

Figure 9 Wind incidence angle by ϒ and ϐ adapted from (Kaplani & Kaplanis, 2014)

Full equations for calculating forced convection coefficient for both sides (h_{forced_fs},h_{forced_bs}) factoring wind speed, direction, incidence angle, kinematic viscosity and characteristic length with parameters check of difference in PV azimuth angle vs wind direction (γ) and air flow condition (laminar, turbulent or mixed) can be referred in the Table 6.

Table 6 Forced convection coefficient equations for PV frontside

Frontside	Forced convection coefficient (h_{forced_fs})	Ref	Eq
$0 \leq \gamma \leq 90$ Or $270 \leq \gamma \leq 360$	$0.848 \cdot k \cdot (\cos(\alpha_w) \cdot v_w \cdot Pr/v)^{0.5} \cdot (0.5 \cdot L)^{-0.5}$	(Kendoush, 2009)	10
$90 < \gamma < 270$ & $\frac{x_c}{L} \geq 0.95$	$3.83 \cdot {v_w}^{0.5} \cdot L^{-0.5}$	(Sartori, 2006)	11
$90 < \gamma < 270$ & $0.05 < \frac{x_c}{L} < 0.95$	$5.74 \cdot {v_w}^{0.8} \cdot L^{-0.2} - 16.46 * L^{-1}$	(Sartori, 2006)	12
$90 < \gamma < 270$ & $\frac{x_c}{L} \leq 0.05$	$5.74 \cdot {v_w}^{0.8} \cdot L^{-0.2}$	(Sartori, 2006)	13

If the ratio $x_c/L \geq 0.95$ the flow is considered laminar, if $x_c/L \leq 0.05$ the flow is fully turbulent and $0.05 < x_c/L < 0.95$ the flow is considered mixed. All wind velocity from backside PV $|\gamma| > 45°$ flowing on PV width with velocity greater than 3 m/s will be considered turbulent regardless the ratio of x_c/L. Flow condition will determine the equation for calculating forced convection coefficient (h_{forced}).

Table 7 Forced convection coefficient equations for PV backside

Backside	Forced convection coefficient (h_{forced_bs})	Reference	Eq
$0 \leq \gamma \leq 90$ Or $270 \leq \gamma \leq 360$ & $\frac{x_c}{L} \geq 0.95$	$3.83 \cdot {v_w}^{0.5} \cdot L^{-0.5}$	(Sartori, 2006)	11
$0 \leq \gamma \leq 90$ Or $270 \leq \gamma \leq 360$ & $0.05 < \frac{x_c}{L} < 0.95$	$5.74 \cdot {v_w}^{0.8} \cdot L^{-0.2} - 16.46 * L^{-1}$	(Sartori, 2006)	12

$0 \leq \gamma \leq 90$ Or $270 \leq \gamma \leq 360$ & $\frac{x_c}{L} \leq 0.05$	$5.74 \cdot {v_w}^{0.8} \cdot L^{-0.2}$	(Sartori, 2006)	13
$90 < \gamma < 270$ & $v_w \geq 3m/s$	$5.74 \cdot {v_w}^{0.8} \cdot L^{-0.2}$	(Sartori, 2006)	13

2.4.3 Combining the free and forced convection

Combining both free and forced convection coefficient to get total convection coefficient is not a simple addition. Since both free and forced convective heat transfer happen at the same time, the ratio of the surface Grashof number (Gr_L) and Reynolds number (Re_L) need to be estimated (Bergman, 2011). Grashof number is related to free convection as Rayleigh number multiplied by Prandtl number in the following equation

$$Gr_L = \frac{Ra_L}{Pr} = \frac{g \cdot cos\theta \cdot \beta \cdot \left(T_{pv} - T_{amb}\right) \cdot L^3}{v^2} \quad \text{(Eq. 14)}$$

Grashof number is related to free convection like Reynolds number is to forced convection. If ${Gr_L}/{Re_L}^2 \ll 1$ the free convection effect may be neglected and conversely, when ${Gr_L}/{Re_L}^2 \gg 1$ the free convection effect can be neglected. Combining the free and forced convection can be considered when $0.01 < {Gr_L}/{Re_L}^2 \leq 100$ (White, 1988) as cited in (Kaplani & Kaplanis, 2014).

To combine the free and forced convection coefficient (h_{c_total}) by following the expression from (McAdams, 1942) as cited in (Churchill, 1977) experiment regarding the correlation between the combined average Nusselt number from forced convection and natural or free convection : $Nu^n = {Nu_F}^n + {Nu_N}^n$ with n = 3 for assisting or opposing fluid flow it can be derived that ${h_{c\_total}}^3 = {h_{free}}^3 + {h_{forced}}^3$ since Nusselt number directly related to convection coefficient in general expression of $h \equiv Nu \cdot k/L$. Since convective heat transfer happen for both PV surfaces at the same time, separate calculations for total convection coefficient are needed. Convection coefficient for PV surfaces can be written in table 8.

Table 8 PV total convection coefficient equations

PV frontside	${h_{c\_fs}}^3 = {h_{free\_fs}}^3 \pm {h_{forced\_fs}}^3$	(Eq. 15.a)

PV backside	$h_{c\_bs}{}^3 = h_{free\_bs}{}^3 \pm h_{forced\_bs}{}^3$	(Eq. 15.b)
PV average	$h_{c\_pv} = \frac{h_{c\_fs} + h_{c\_bs}}{2}$	(Eq. 16)

The plus / minus (±) sign depends on whether the forced convection is assisting or opposing the natural free convection. Meaning that if the forced convection flow is assisting the free convection flow the sign is positive (+) and if the forced convection is opposing the free convection flow the sign is negative (-). The sign considers PV orientation vs wind direction (γ) upwind or downwind, and PV operating state whether as a hot plate or cold plate. The illustration is in the following figure.

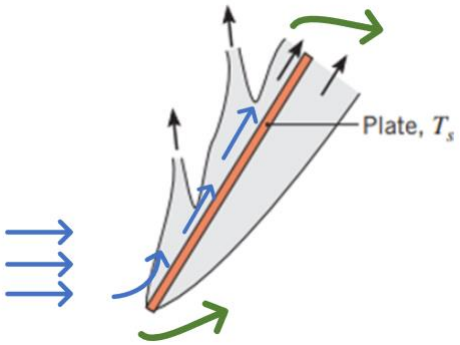

Figure 10 Combination of free and forced convection for upwind PV frontside as a hot plate

The PV from Figure 10 operates as a hot plate ($T_{pv} > T_{amb}$), the free / natural convection flow (black arrows) will be from bottom (leading edge) to top (trailing edge) and since the frontside is upwind, the flow from forced convection which is wind (blue arrows) is assisting the free convection. On the same time, the backside of the PV is downwind (green arrows), the flow of the forced convection especially from the bottom and top of the PV is on the relatively same path with the free convection, this condition is the same even if the flow on PV backside is turbulent, thus the combined convection coefficient sign is plus (+). With the same concept, when PV in in a cold plate state ($T_{pv} < T_{amb}$) if the frontside is upwind the free convection flow from the top of the PV to the bottom and is against by the forced convection, hence the flow is opposing each other resulting the sign is minus (-). The relation of the sign for the PV front side can be referred to in the Table 9.

Table 9 Combined convection coefficient sign for upwind PV frontside

PV State	PV Side	Sign
Hotplate	Frontside	+
Hotplate	Backside	+
Cold plate	Frontside	-

Cold plate	Backside	+

Illustration for upwind PV backside as follows

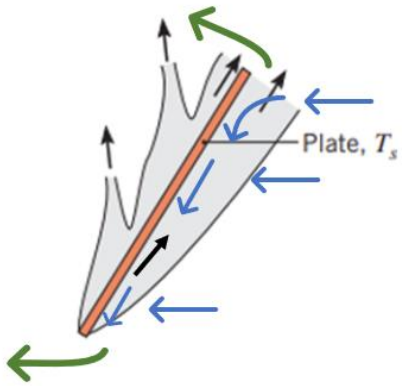

Figure 11 Combination of free and forced convection for upwind PV backside as a hot plate

If the backside of the PV is upwind, Figure 11, the flow from free convection (black arrow) will be opposed by flow from forced convection (wind), thus the sign will be (-). Since the forced convection (wind obstructed by PV) is assisting the natural convection on the frontside the sign will be (+). Operating in cold plate state, with the same logic, when backside PV is upwind the sign will be (+). A note for upwind PV backside is if the velocity is greater than 3 m/s the flow of forced convection on the frontside is considered turbulence. A turbulence flow means the rate of moving fluid is faster resulting in a higher convection coefficient. Table 10 is the sign for flow on upwind PV Backside

Table 10 Combined convection coefficient sign for upwind PV backside

PV State	PV Side	Sign
Hot plate	Backside	-
Hot plate	Frontside	+
Cold plate	Backside	+
Cold plate	Frontside	+

Since we are assuming that both PV surfaces have the same temperature, which means no conductive heat transfer, the convection coefficient for the whole PV module can be estimated as the average of the frontside and backside convection coefficient (Eq 16).

3 Methodology

3.1 Site data processing and software selection

Planned to be built in Tennant Creek Australia, Sun Cable's utility-scale solar farm with 13 GWp capacity can be considered as one of the largest PV solar farms in the world. The solar farm will be supplying approximately 20% of Singapore electricity which mainly comes from natural gas. Data processing for the solar farm location becomes an essential task to see whether the location is operational and financially feasible. Long term annual solar and weather data are provided by Sun Cable Pte. Ltd from (Solcast, 2021). From data processing it is expected to get the convection coefficient for predicting solar PV output including sensitivity analysis to get a more accurate energy yield forecast. Analyzing the convection coefficient can be very important since it can affect PV performance in terms of efficiency and lifetime.

To model the PV convective heat transfer both ambient and PV temperature is needed thus, and because PV temperature is highly determined from solar irradiance, solar data processing becomes inevitable. Wind data characteristics are needed for factoring the wind speed and direction into convection coefficient equations. Data being analyzed in this thesis is a forecasted meteorological data such as hourly solar irradiance (DNI, GHI, DHI), solar zenith, solar azimuth, ambient temperature, wind speed and wind direction. Since the data is hourly based then there will be 8760 of data timestamps for one year and since the calculation is not too complex the software being used is Microsoft Excel which is an easy-to-use tool but quite capable for simple data processing and sensitivity analysis.

The methodology for this thesis is divided into four parts: the first part is solar data processing to get the general condition of solar irradiance and for setting the right PV inclination angle. Second part is Wind parameter characteristics to get a clear picture of wind conditions in the area. Third part is PV convection modelling explaining the steps how the model is constructed by factoring every data and parameters that are being used. The last part is explaining an example of designing a utility-scale solar PV farm using Helioscope, a web-based PV application.

3.2 Solar data processing & Optimum tilt angle

3.2.1 DNI, DHI, GHI

Solar and PV data processing main objectives are for estimating annual, average, daily solar irradiation, also maximum, and minimum solar irradiance in the farm location. This becomes an integrated factor for energy yield forecasting since more solar irradiances translate to more energy. High average Irradiance doesn't always mean higher energy yield because if the irradiance goes very high but only for a relatively short time, this means that the location has a wide gap between maximum and minimum irradiance and has a bigger risk of more PV electrical power output being curtailed. For this type of location, a further investigation regarding shadowing, soiling, or other losses needs to be conducted.

The second objective of solar and PV data processing is because PV performance whether its power output and lifetime are highly related to PV operating temperature, and since high irradiance translates to higher temperature choosing the right PV will be beneficial for the solar farm. Selecting PV by matching the thermal constants with the location irradiance profile is to estimate the PV operating temperature, which will be related with the temperature to efficiency coefficient. After all PV parameters are being decided, combined calculation of PV and solar data become more relevant and will be site-specific. Important parameters for this data processing are DNI, DHI, GHI, EBH, GTI and ambient temperature. The above important terminologies from (Solcast, 2021) are Direct normal irradiance (DNI) is solar irradiance received on a surface perpendicular to the sun. DHI is irradiance from the sun scattered by the atmosphere as a horizontal component or diffuse horizontal irradiance. Global horizontal irradiance (GHI) is total irradiance received by horizontal surface, means a flat plate, and is a sum of DHI and EBH or direct beam horizontal irradiance. Even though these terminologies seem common, apparently many sources give different definitions, usually defining that GHI is the sum of DNI and DHI.

3.2.2 Optimum tilt angle

Annual solar data is grouped using Excel PivotTable function based on hourly average for every month to get solar irradiance profile in the area. Since in this thesis only consider fixed racking system angle of incidence (AOI) between PV plane of array (POA) and the sun need to be calculated with the following equation (Sandia, 2018).

$$AOI = cos^{-1}[\cos(\theta_Z) \cdot \cos(\beta) + \sin(\theta_Z) \cdot \sin(\beta) \cdot \cos(\gamma_S - \gamma_{pv}) \quad \text{(Eq. 17)}$$

Where θ_Z is solar zenith angle, γ_S is solar azimuth and γ_{pv} is POA azimuth. From the above equation, in theory, optimum tilt angle can be calculated by finding maximum $\cos(AOI)$. Fixed racking system only considers one value of β, which will be used during solar farm construction. Optimum tilt angle (β_{opt}) is that it receives solar irradiance the most throughout the year. The optimum tilt angle, being calculated from series of data using (Eq. 17) since solar zenith and solar azimuth data is already being provided and POA azimuth is set to 0^o or due north because the farm location is on the southern hemisphere. In this thesis multiple experiments for different inclination angles are being conducted in the series of sensitivity analysis (chapter 4) and the result is being compared with calculation and conformed with popular applications such as: (globalsolaratlas, 2021). Optimum tilt angle will be used to calculate total optimum POA irradiance or Global Tilt Irradiance (GTI) as the primary energy source for PV solar farms (World Bank, 2017). The GTI is calculated by using by the following equation (Sandia, 2018).

$$GTI = DNI \times \cos(AOI) + DHI + Ground\ Reflected \quad \text{(Eq. 18)}$$

The average hourly solar data for every month can be referred to in the Annex. The GTI in some timestamps provided by Solcast gives a solar zenith angle greater than 90 meaning that the sun is yet to rise, thus often

in this condition the solar irradiance is 0. For zenith angles close to 90, usually small irradiance from DHI or EBH are detected and being used for GTI calculation.

3.3 Wind characteristics

Two important wind parameters will be processed for convective heat transfer, that is wind speed and wind direction. In the same direction, wind has different speeds for different height and terrain roughness. Terrain roughness implies a vertical height that can obstruct the wind flow, the rougher the terrain the more protrusion of the wind in the area. Sun Cable proposed the PV solar farm to be in an open flat terrain with only a few obstacles.

There is a height difference where the wind is measured with PV pole height. The wind is measured at 10 m height while PV pole height is assumed to be 2.5 m. The wind speed equation for estimating wind speed at different altitudes (WMO, 2008).

$$v_1 = v_{ref} \cdot \frac{\ln(\frac{h_1}{z_0})}{\ln(\frac{h_{ref}}{z_0})} \qquad \text{(Eq. 19)}$$

Where v_1 is wind speed at PV height (h_1) and v_{ref} is wind speed measured at h_{ref}. z_0 is location roughness length. For flat open terrain, see Figure 12, the roughness length estimated to be 0.03 (WMO, 2008)

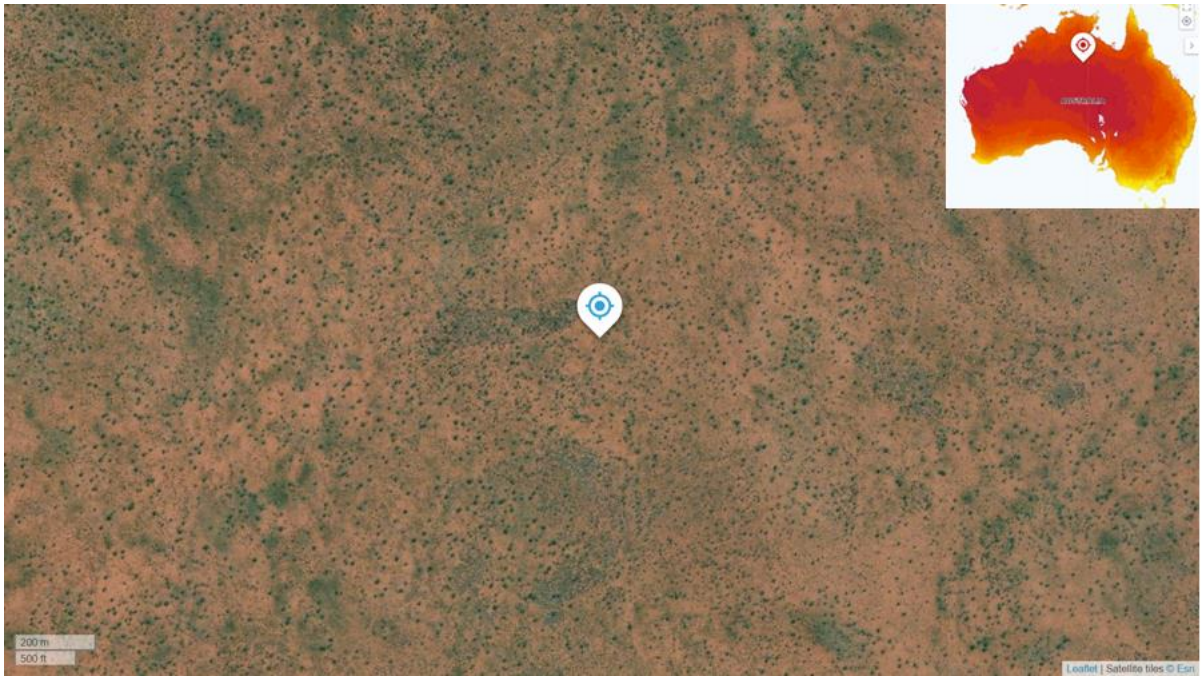

Figure 12 Terrain profile of the proposed solar farm image by (ArcGIS, 2021) scale 1:200,000

After calculating the wind speed at PV height then the wind data is grouped by its direction angle in 16 sectors with 0^o as the north and charted in the wind rose diagram. The wind rose diagram shows the frequencies of occurrence for a range of wind with its magnitude and direction. The sector group range as referred by (NNDC, 2021) is on Table 11.

Table 11 Wind sector grouping

Abbreviation	Description	Angle (degrees)
N	North	349 – 011
NNE	North-Northeast	012 – 033
NE	Northeast	034 – 056
ENE	East-Northeast	057 – 078
ESE	East-Southeast	102 – 123
SE	Southeast	124 – 146
SSE	South-Southeast	147 – 168
S	South	169 – 191
SSW	South-Southwest	192 – 213
SW	Southwest	214 – 236
WSW	West-Southwest	237 – 258
W	West	259 – 281
WNW	West-Northwest	282 – 303
NW	Northwest	304 – 326
NNW	North-Northwest	327 – 348

Grouping and creating the wind rose diagram for better data visual interpretation is by using Microsoft Excel Pivot Table and can be referred to in the annex.

3.4 PV convection modelling

In this section the convective heat transfer model is being constructed by calculating the free and forced convection and the combining process.

3.4.1 PV free convection modelling

In free convection, parameters to be checked are critical Rayleigh number, inclination angle (β), operating state (hot or cold plate), and flow characteristic (laminar or turbulent). The model output is the free convection coefficient for both PV sides by calculating average Nusselt number. PV temperature is necessary for calculating the Rayleigh number. The Estimation of PV temperature obtained by using (Faiman, 2008) equation (Eq. 1) with GTI (Eq. 18) as the *H*. The expression will be

$$T_{pv\_ts} = T_{amb\_ts} + \frac{GTI_{ts}}{U'_0 + U'_1 \times v_{w\_ts}} \quad \text{(Eq. 1.a)}$$

Where GTI_{ts}, T_{pv_ts}, T_{amb_ts}, and v_{w_ts} are the corresponding time stamped Global Tilted Irradiance, PV, and ambient temperature. PV *U* value is provided by Sun Cable for PV with U'_0 = 25 (W/m^2 K) and U'_1 = 1.2 (W/m^2 K / m/s). PV temperature determines the PV operating mode, thus determining the free convection flow. If $T_{pv} > T_{amb}$ then the PV operates as a hot plate and conversely, if $T_{pv} < T_{amb}$ then the PV is operating in cold plate mode. The PV Rayleigh number equation is calculated with (Eq. 2) with the air thermal diffusivity (α) and kinematic viscosity (ν) corresponding with its temperature. The value for α and ν can be consulted in the table of air properties at 1 atm pressure at the Annex A.3. The value of important air properties that are not mentioned in the table is approached by linear or polynomial regression using Excel trendline function.

Critical Rayleigh number is calculated with $\theta = 90 - \beta$ thus, the expression as follows

$$Ra_c = 10^{8.9 - 0.00178 * (90 - \beta)^{1.82}} \quad \text{(Eq. 20)}$$

where β is in degree. The last step for free convection modelling is for estimating the average Nusselt number equation for both PV sides. Since all parameters are known, a suitable average Nusselt number equation can be chosen. With the assumption that the PV operates as a hot plate, turbulent flow, and low inclination angle ($\beta < 30$) then the average Nusselt number for PV front side can be obtained by using (Eq. 5) and for back side uses (Eq. 7). Free convection coefficient is directly related to average Nusselt number by $h \equiv N_u \cdot k/L$ where k is air thermal conductivity (W/m. K) at corresponding temperature.

The flowchart for calculating free convection coefficient, as previously explained, can be referred in the Figure 13

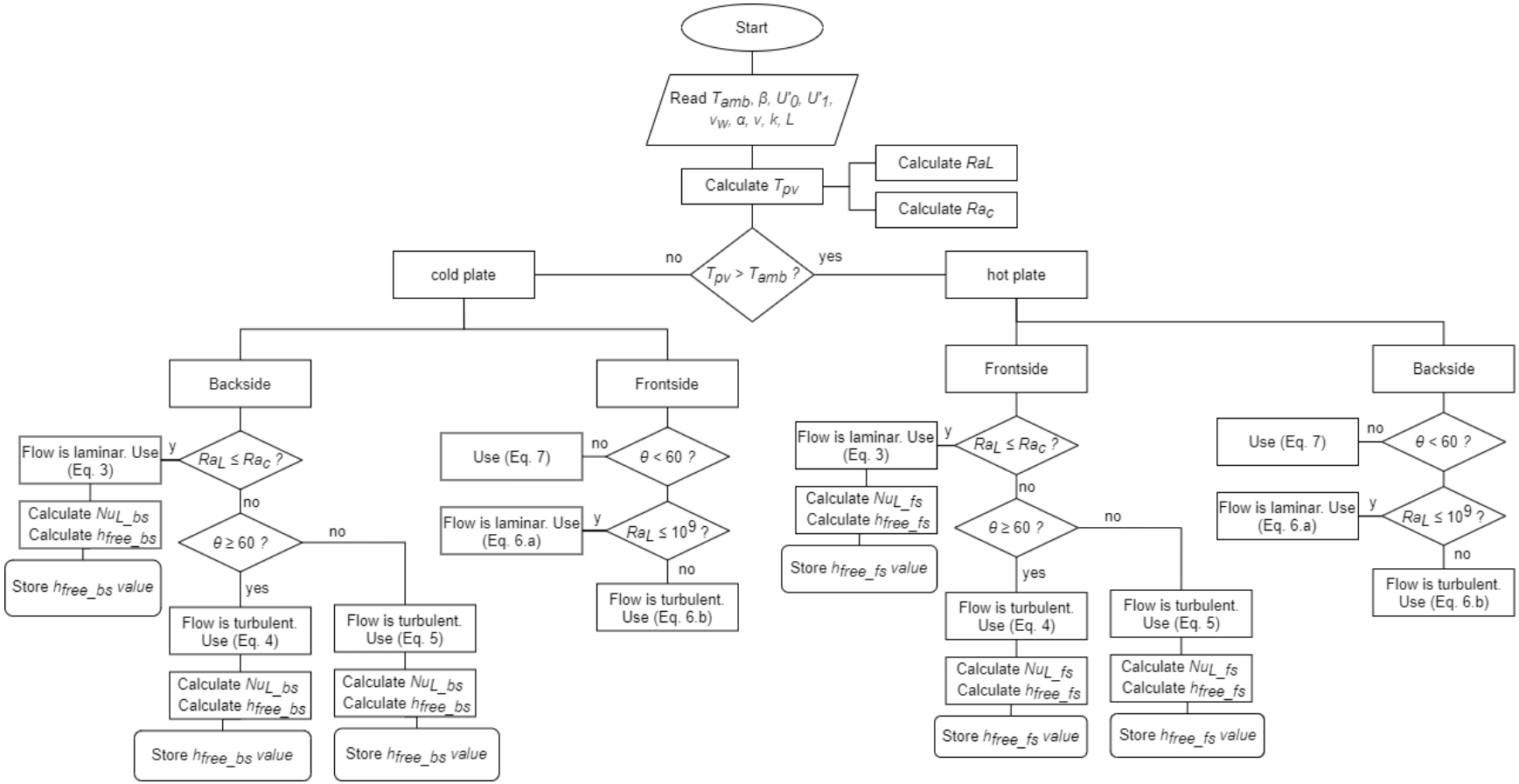

Figure 13 Free convection flow chart

3.4.2 PV forced convection modelling

PV forced convection model checking parameters are wind direction (Y_w), wind speed (v_w), PV azimuth (Y_{pv}), surface characteristic length (L), PV inclination angle (β). The value of L depends on angle between PV azimuth and wind direction (Y) is calculated by $\gamma = |\gamma_{pv} - \gamma_w|$. Since the PV azimuth is due north (0 degree), for upwind PV side if 45<Y <135 or 225<Y<315 then the L is the PV width since the wind is travelling on the width. Using the same concept, L equal to PV height If upwind PV side Y ≤45 or 135≤Y ≤225 or 315≤Y≤360. For downwind PV side $L = 4 \cdot A/S$ where A is PV surface area ($A = H_{pv} \times W_{pv}$) and S is PV perimeter ($S = 2 \times (H_{pv} + W_{pv})$). For upwind calculation wind incidence angle (α_w) needs to be calculated from $\alpha_w = cos\ (\gamma) * \cos\ (90 - \beta)$.

The flow characteristic for both PV sides can be check by calculating the surface critical length

$$x_c = Re_{x,c} \cdot \upsilon / v_w.$$

Where υ & v_w are air kinematic viscosity and wind speed, $Re_{x,c}$ ≈ 4 x 10^5. Choosing forced convection coefficient (h_{forced}) equation for both PV sides are depending on the ratio of x_c / L. if (x_c / L) ≥ 0.95 the calculation will be based on (Eq.11) and for 0.05 < (x_c / L) < 0.95 (Eq.12) will be used and if (x_c / L) ≤ 0.05 the equation is (Eq.13). For upwind side (Eq 10) is used except for one special condition when PV backside is upwind, flow travelling on the width, and the wind speed is higher than 3 m/s then the convection flow is considered as turbulent regardless of x_c / L ratio and (Eq. 13) is used. The flow chart for forced convection modelling can be referred in Figure 14

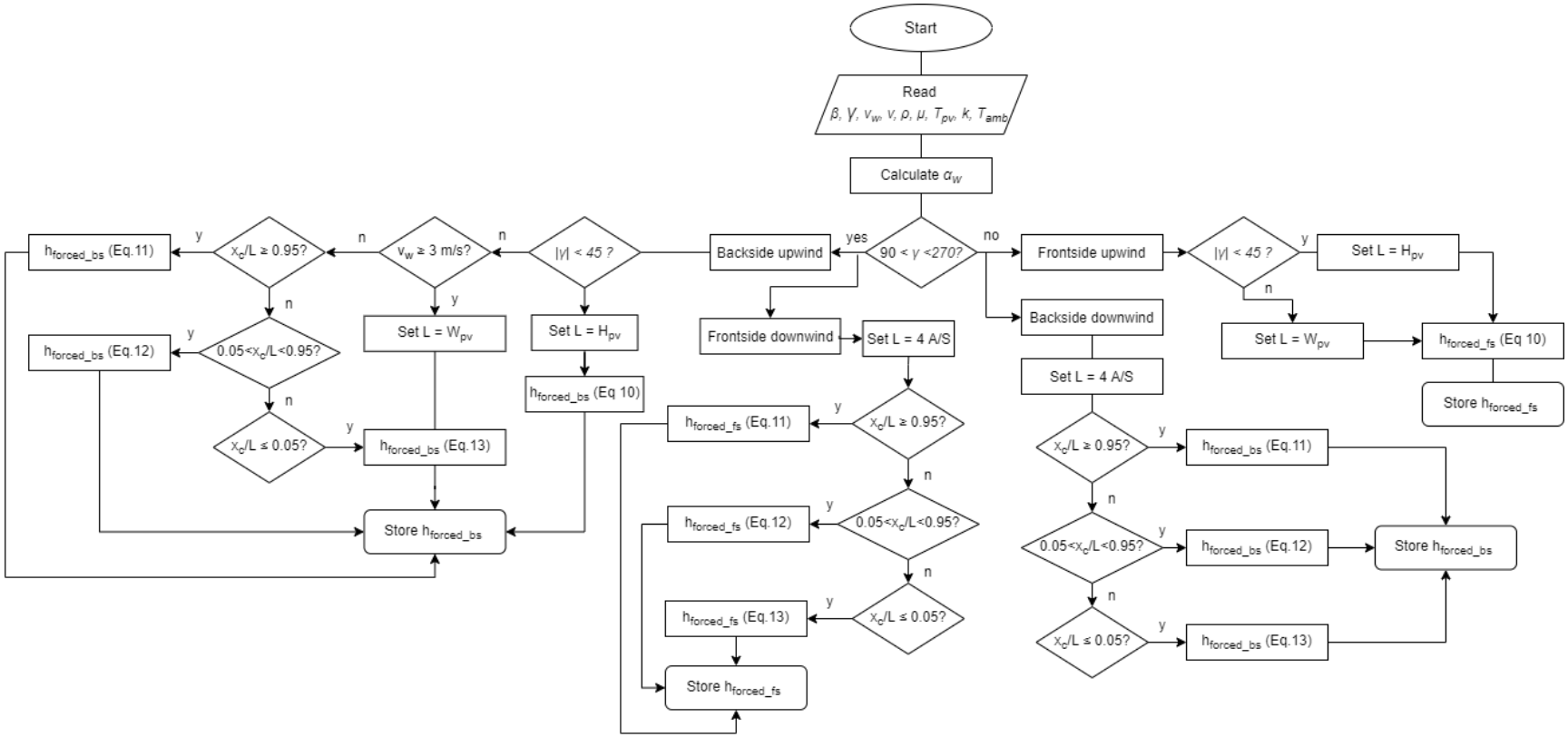

Figure 14 Forced convection flow chart

Checking parameters for combining free convection and forced convection are the Grashof and the Reynolds number ratio. For $Gr_L/{Re_L}^2 \leq 0.01$ the total convection coefficient (h_c) is only determined by forced convection (h_{forced}), and for $Gr_L/{Re_L}^2 > 100$ only free convection is considered. Mixing free and forced convection is when $0.01 < Gr_L/{Re_L}^2 \leq 100$.

Complete combined convection coefficient with the checking parameters in Figure 15.

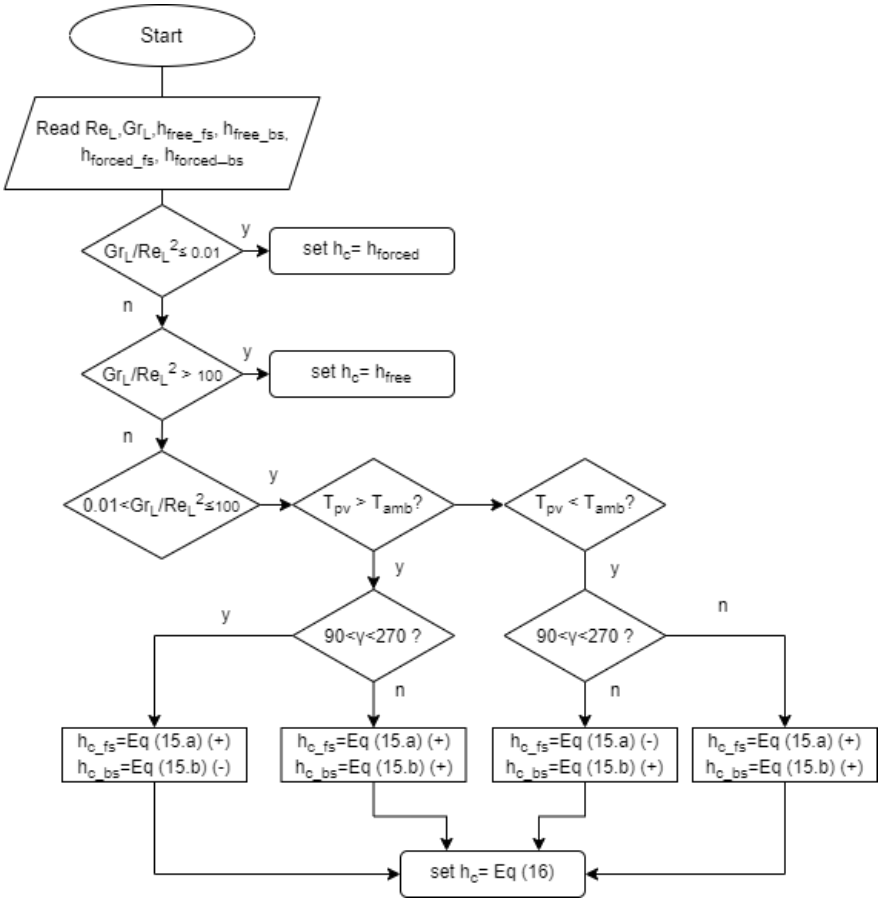

Figure 15 Flowchart of combined convection

3.5 Solar farm modelling in Helioscope

Helioscope is a cloud-based software to design solar PV systems for small scale residential PV rooftop, commercial PV arrays systems, and utility-scale ground mount PV solar farms. Hourly annual energy production can also be simulated using Helioscope, including system performance and losses, which enable us to evaluate each detail design decisions.

The modelling starts with initial input of location address or latitude and longitude of the solar PV farm, then specifies the designated area and the keep out zone. Helioscope has some default input parameters and will automatically generate PV arrangement layout, default recommendation PV module and inverter, and

wiring diagram. The information about tilt angle and azimuth angle of PV module, maximum installed PV system capacity, height, row spacing, PV module orientation layout, PV module frame size, racking, etc. can also be determined refer to preliminary design. Designers can choose the required PV module, inverter, and cabling size. Technical specifications of chosen equipment will be automatically adapted into the system model. Unlike other PV design tools. See Figure 16 for sample of 1 MWp modelling, the blue boxes are PV solar panes while the blue circle in the middle represents the inverter.

Helioscope calculates mismatch losses, DC wiring losses depending on the designs, instead of using default values. In order to get maximum possible energy production and better performance ratio, system Losses report and shading report can be used to evaluate the technical design and layout arrangement.

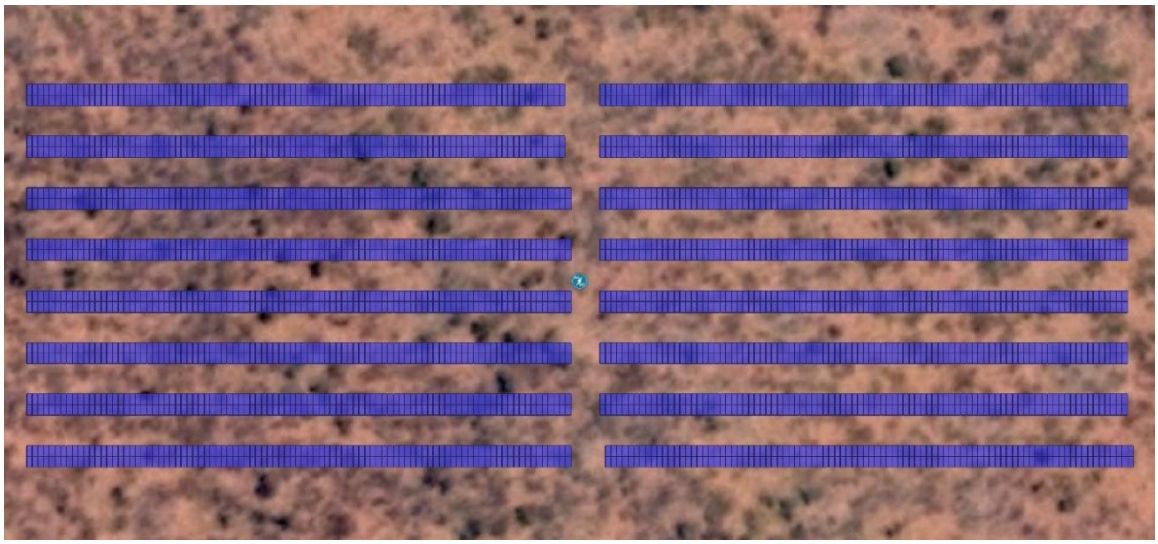

Figure 16 Sample of helioscope modelling 1MWp Solar Farm

4 Results & Discussion

4.1 Solar data & PV analysis

4.1.1 Solar data analysis

Solar irradiance data provided by Sun Cable shows that the PV farm location has annual DNI solar potential of 2.49 MWh/m^2 and GHI is 2.28 MWh/m^2. With a ratio of GHI/DNI ≈ 0.92, it suggests that the location is suitable for lower PV inclination angle (β) < 30^o. As mentioned before, the minimum β that will be considered in this thesis is 2^o this is to combat soiling and increase PV self-cleaning. Optimum β is calculated by sensitivity analysis of the irradiance data using (Eq. 18) with Excel Data Table function.

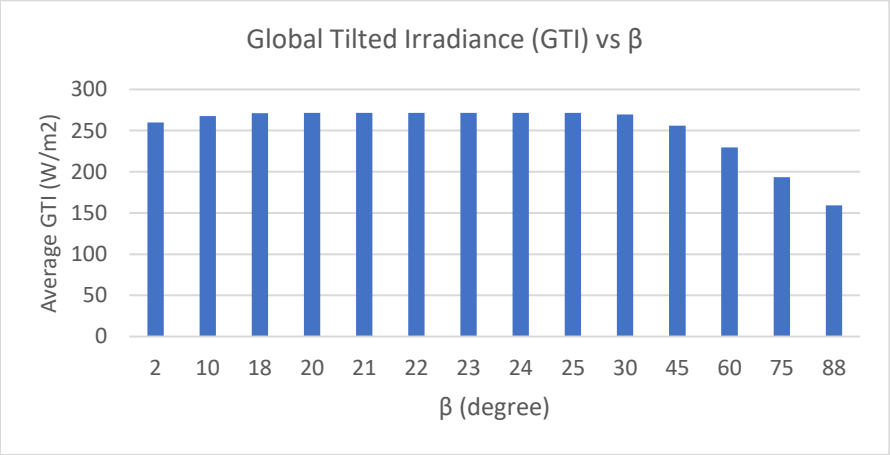

Figure 17 Sensitivity analysis of GTI vs PV inclination angle (β)

The data chart on Figure 17 indicates that the POA will receive good solar irradiance for smaller β. Optimum inclination angle ($\beta_{optimum}$), which gives maximum GTI, is ≈ 22^o this is aligned with Figure 1 from (globalsolaratlas, 2021). The chart also indicates that for 2 < β ≤ 30 the irradiance difference is less than 5%. For β above 30 the GTI starts to decline suggesting that to operate the PV farm using these β is not favorable. Comparison between the model GTI and GTI from Sun Cable data in the figure below shows the model variance ≈ 2% for small irradiance (100 W/m^2<) and less than 0.5% for higher Irradiance (250 W/m^2++) on Figure 18.

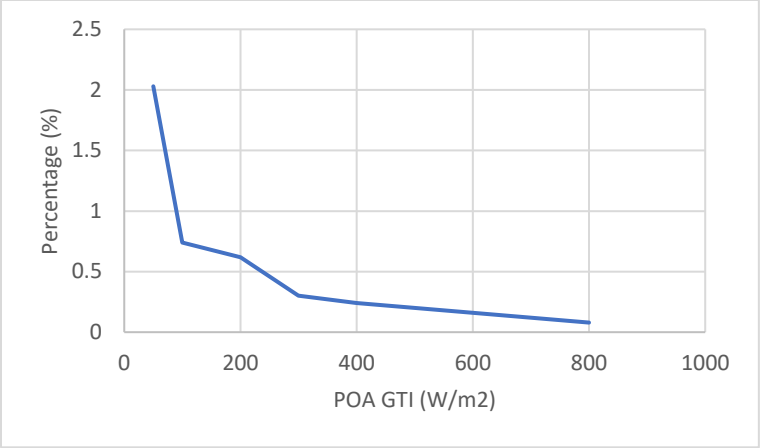

Figure 18 GTI Variance model vs POA

4.1.2 PV Module Analysis

The Assumed PV module to be installed in the solar farm is JAM72S10 400 PR from JA Solar with the range of operating temperature from -40^{o} to 85^{o}C and NOCT 45 ± 2^{o}C. The PV module has a height of 2.015 m, width of 0.996 m and temperature coefficient of maximum power -0.35%/^{o}C. From data calculation, the POA will receive average GTI during daytime of 503 W/m^2 with maximum GTI 1100 W/m^2. Calculation result for PV temperature using (Eq. 1) indicating the maximum PV operating temperature estimated to be 78^{o}C which is still in the PV module operating range. The average T_{PV} is 35.4^{o}C. means on average the PV will lose -0.35 * (35.4 – 25) = 3.65% from its rated maximum power output. The cumulative probability of PV operating temperature is on Table 12.

Table 12 Cumulative probability PV operating temperature

Tpv > (°C)	Cumulative probability
25	72%
30	52%
35	40%
40	33%
45	28%
50	22%
60	11%
70	2%

The free convection coefficient (h_{free}) for both PV sides on Figure 19 suggested the PV mostly operates as a hotplate this is because the frontside free convection coefficient (h_{free_fs}), the grey line, is higher than backside (h_{free_bs}), the green line. Along with the increasing inclination angle, the free convection flow behavior of PV is becoming more to that of vertical plate, thus having the same value for both sides. As previously mentioned, that β above 30^{o} is not advisable, the chart is only for showing that the model is still consistent with the theory even when using different equation for frontside and backside.

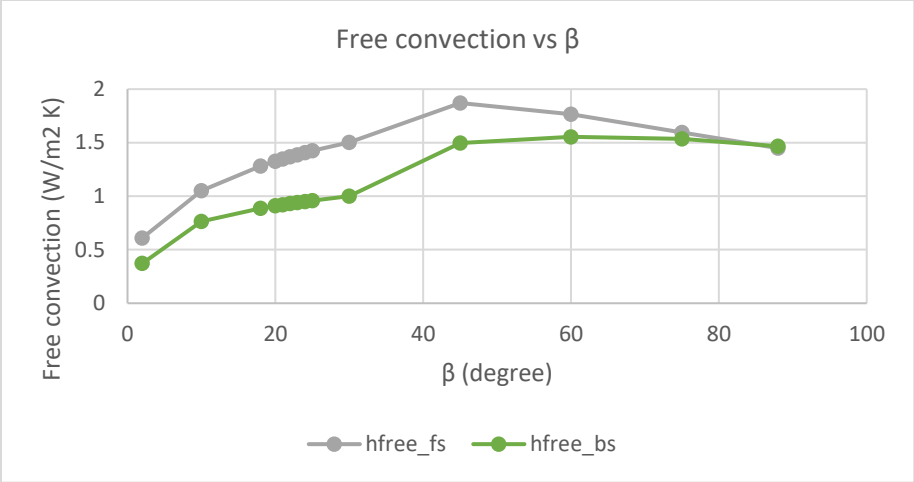

Figure 19 Free convection coefficient PV front and backside vs inclination angle

4.2 Wind analysis

Wind data analysis is needed to see the general condition of the wind. Parameters being processed are wind speed and wind direction. By using (Eq. 19) The site average wind speed is 3.63 m/s at PV height of 2.5m. Wind grouping along with the probability is charted on a wind rose diagram (Figure 20).

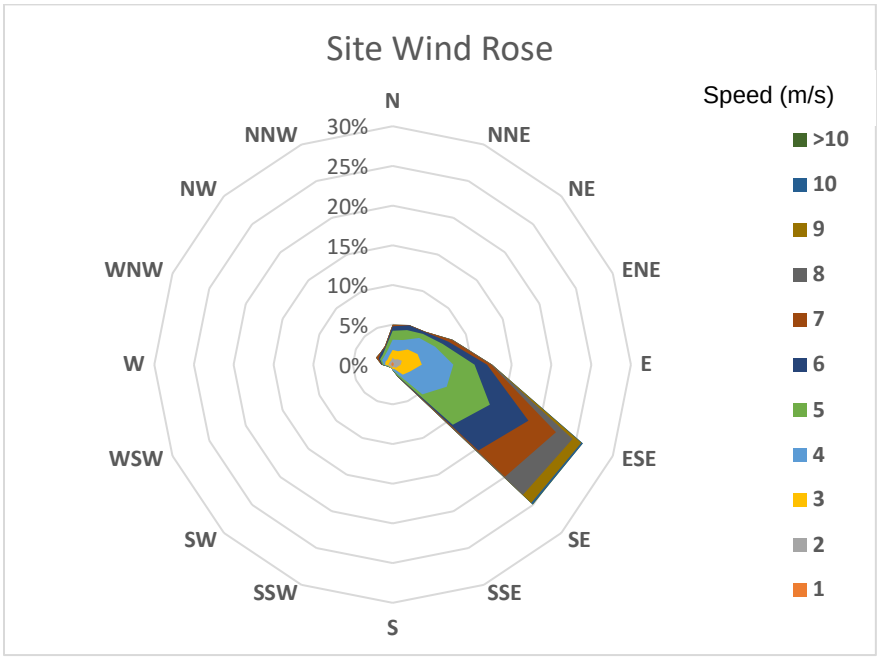

Figure 20 Wind rose diagram of the PV solar farm

Wind direction characteristic at PV height is dominant with wind flow from southeast and east-southeast direction. The forced convection for both PV frontside and back side (h_{forced_fs}, h_{forced_bs}) corresponds with the inclination angle as follows in Figure 21.

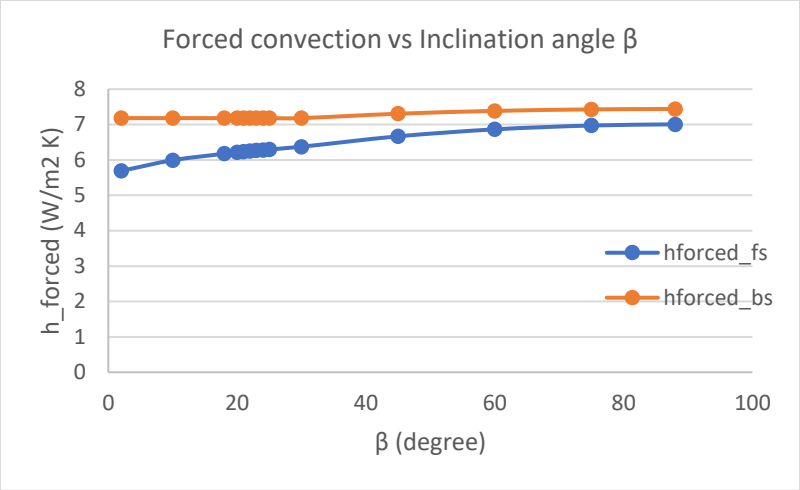

Figure 21 Forced convection on PV sides vs Inclination angle

Backside forced convection is higher than the frontside since the dominant wind comes from PV backside. Higher inclination angle means more wind incidence to the surface and translates to higher convection. Higher inclination tends to obstruct the wind flow, thus tends more turbulent to downwind side, and for this case the downwind side is mostly the front (blue line) thus forced convection coefficient on frontside tends to be higher for high inclination angle. Comparing forced convection and free convection, from both charts the forced convection coefficient is higher than the free convection coefficient, thus playing a bigger role in the overall convective heat transfer.

4.3 Convection coefficient sensitivity analysis:

4.3.1 Convection coefficient vs PV Inclination angle

Series of sensitivity analysis being conducted, in Figure 22 and Figure 23, with the main goal is to get the relation between overall convection coefficient (h_c) with β and γ. Convection coefficient increases as β increases since both forced and free convection coefficients also increase. This model shows a relation that total convection coefficient $h_c \approx h_{forced} - h_{free}$. This is because mostly PV is operating as a hot plate and PV backside is upwind since dominant wind comes from the backside.

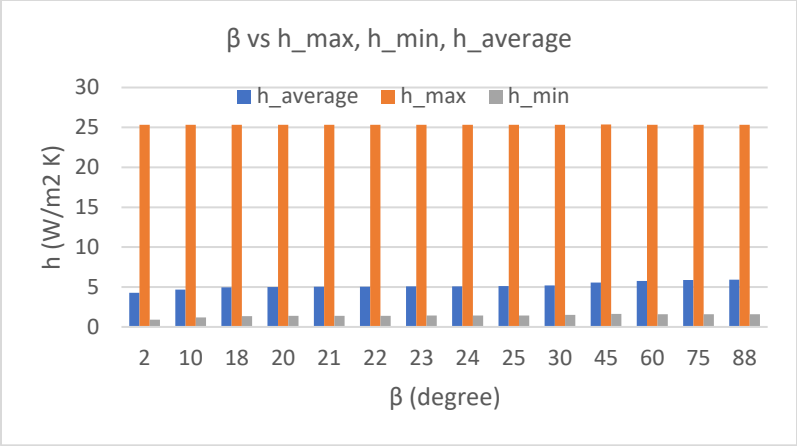

Figure 22 Maximum, minimum and average convection coefficient vs β

The average convection coefficient for optimum β is 5.1 W/m^2 K

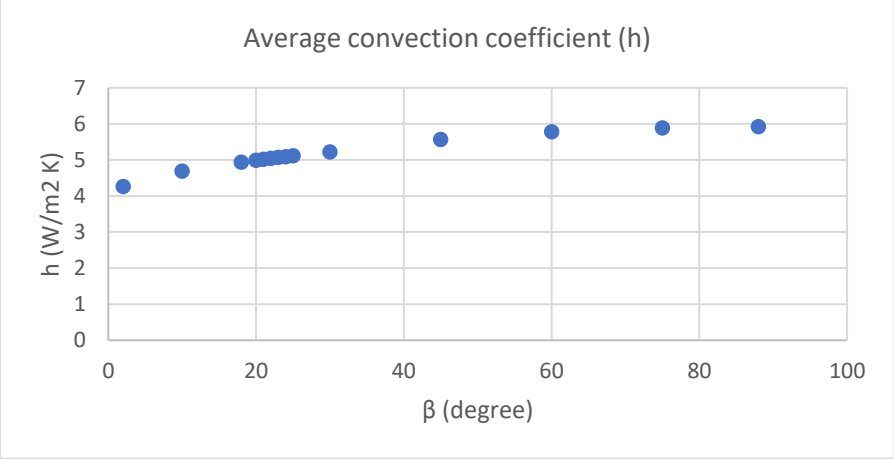

Figure 23 Average convection coefficient

4.3.2 The effect of wind direction to convection coefficient

This sensitivity analysis, comparing h_c vs γ in Figre 24 is being conducted by grouping the wind direction into a certain degree but keeping other parameters constant. From the chart the lowest h_c is 2.8 W/m^{2}K, happens when the wind is blowing in a small angle from west or east of the PV surface. This is possibly because the wind flow is not obstructed or tends to be laminar and has a smaller Nusselt number by having a short characteristic length (L). The highest average hc is 7.5 W/m^{2}K obtained if all the wind comes from south (180 degree) or upwind PV backside. With the same wind speed h_c can increase to almost 50% if the direction changes to the most optimum.

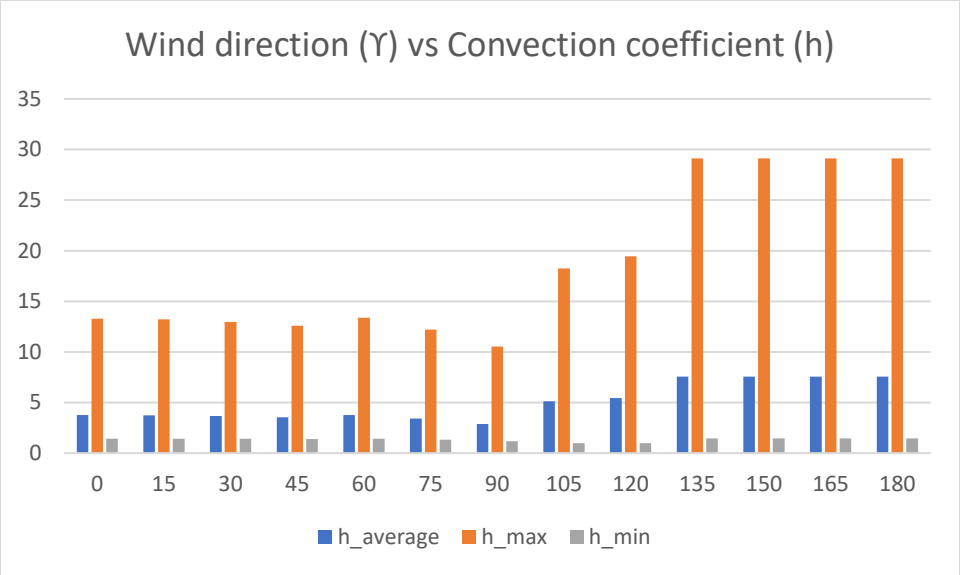

Figure 24 Wind direction vs convection coefficient

4.3.3 Wind velocity and convection coefficient

Another important parameter is the wind speed. The chart signals that the wind speed also affects convection coefficient significantly since the forced convection equation depends on wind speed. Below is the relation of wind speed and h_c if the wind speed is changed while keeping other parameters constant h_c will also increase almost exponentially especially when temperature is high (Figure 25).

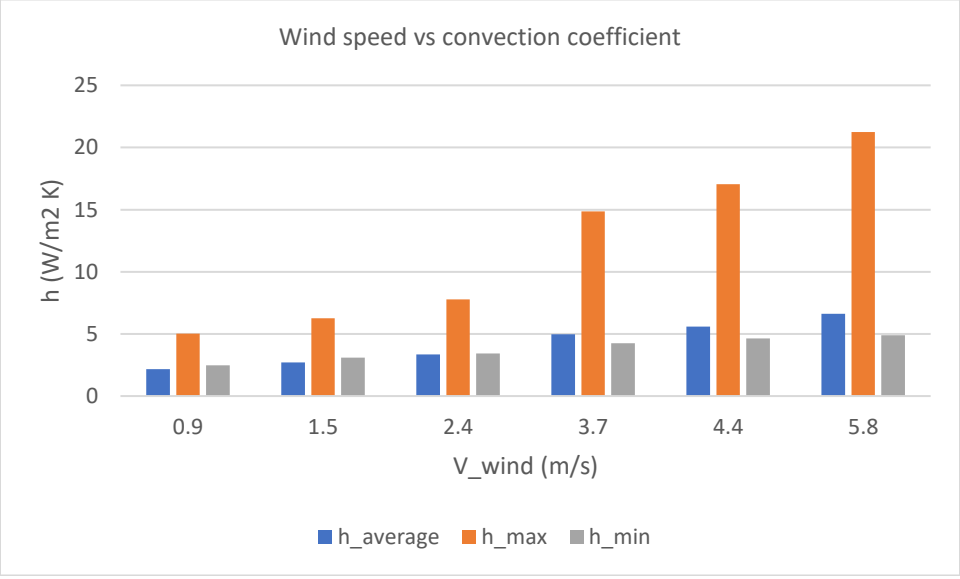

Figure 25 Windspeed vs convection heat transfer

From series of sensitivity analysis and by using newton general expression on heat transfer (cooling) $Q = h \cdot (T_{PV} - T_{\infty})$ if we compared the PV temperature difference between this thesis PV convection model with the same but disregarding the wind direction, the temperature difference estimated to be 2.37°C and since

the PV temperature coefficient for P_{max} for the assumed PV is -0.35%/^{o}C this temperature difference translates to 0.83% difference in efficiency.

4.4 PV solar farm layout recommendation

Passive convection cooling should be taken advantage of to design PV solar farm, by considering wind direction, without sacrificing optimum azimuth and tilt angle. Based on (Glick & Ali, 2020) experiment regarding PV arrangement, to maximize the wind direction that converges started from 8 – 9th row, an example of 1 MWp PV solar farm layout recommendation and designed by using Helioscope as in Figre 26.

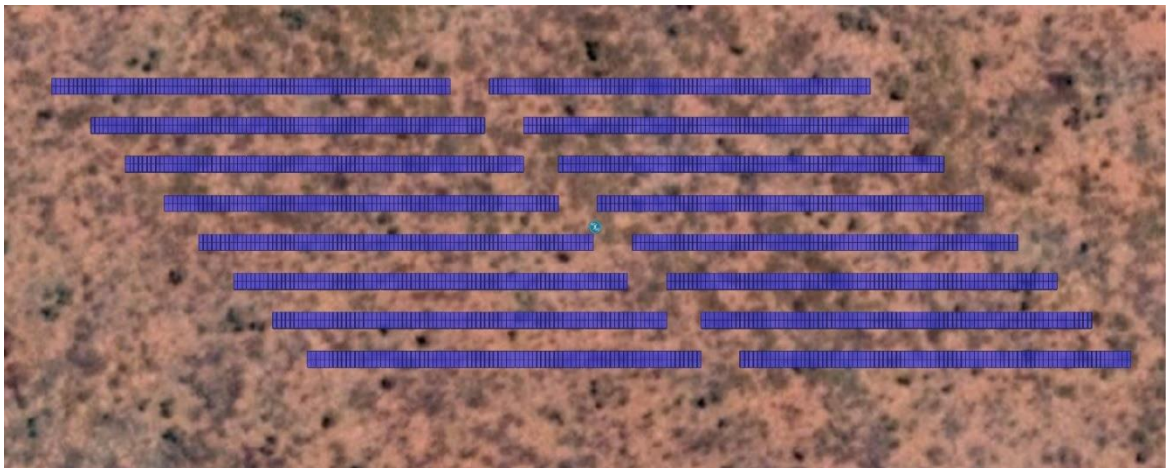

Figure 26 Proposed 1 MWp solar farm layout

The solar farm consists of approximately 2888 PV JAM72S10 400 PR modules, 1 MWp solar inverter, with maximum capacity of 1,1 MWp. If -2% soiling is considered, the annual energy yield at irradiance level forecasted to be 2,590 MWh, the Helioscope annual production report can be referred in Annex A.5.

4.5 Economical & environmental impact

The 0.83% difference in efficiency will be calculated to estimate PV solar farm output at cell temperature. If wind convection is disregarded the temperature will cost -7.7% from energy yield. By accommodating this model, the loss can be cut up to -6.87% or save 21.45 MWh of electrical energy. On a global scale, a typical household with standard appliances consumes 1,250 kWh annually (IEA, 2020) this means the saved energy can potentially provide for 17 households. Economically, Sun Cable will sell the electricity to Singapore, and by considering the selling price to Singapore is 0.1 USD / kWh (globalpetrolprices, 2021) or 0.086 Euro/kWh assuming ratio USD to Euro is 0.86. This energy saving can be up to 1,845 Euro. In terms of environmental effect, if the energy is supplied by natural gas power plants, which 80% of Singapore power plants, has an approximate CO_2 emission of 488 gCO_2eq/kWh (Parliament, 2011) then the annual emission will be 10,467 kg CO_2eq. If the social cost of carbon, a measure of socio-economic harm because of damages from one ton carbon dioxide emission, is 50 USD or 43 Euro per ton (EDF, 2015) the annual social carbon cost will be 450 Euro.

This number scales up with the solar farm capacity. Sun Cable planned to build more than 13 GWp capacity of PV solar farm and send 2GW to Singapore. With the assumption that only for 2GWp with increased efficiency, the energy saving now will be more than 42,900 MWh, equal to almost 3.7 million Euro and can provide for more than 34,000 households also potentially reduced 20,934 kiloton CO_2eq annually and the annual social cost of carbon that can be avoided will be more than 900,000 Euro.

5 Conclusion & Future Work

The most ideal solar PV farm site should be in a location where there is abundant solar irradiance, lower ambient temperature, high wind speed from PV backside direction and has a high optimum inclination angle. It is quite an “impossible” task to find a location that ticks all the boxes, while the electricity demand is getting higher, and more utility-scale solar farms are being constructed every year to fill that demand. Therefore, the study of wind effect: speed and orientation in enhancing PV performance can be considered as an additional value in forecasting PV solar farms output.

In terms of convection coefficient (h_c), a location with higher h_c means higher heat exchange from PV surface to the fluid (air), this resulting less temperature difference between PV temperature and ambient temperature thus, lower PV temperature and results in higher electrical power output. Both free and forced convection for PV front and backside with their respective flow characteristics need to be accommodated in h_c calculation. Optimum PV tilt angle against solar irradiance and convection heat transfer need to be considered to obtain maximum energy yield. Prioritizing optimum PV tilt angle and azimuth is needed for obtaining best possible solar irradiance. Finding a solar farm with good wind speed and dominant wind direction from PV backside is preferred to get better PV performance. For this thesis location the efficiency is higher 0.83% compared if we disregard the wind direction.

This convection model can benefit for PV solar farm developers in giving a more complete analysis compared to the traditional model especially in a farm located in high latitude which will have higher optimum inclination angle and strong wind. A small increase of efficiency and lower PV temperature in a utility-scale solar farm means a large additional electrical energy and longer PV lifespan thus, can reduce capital expenditure for deploying a lesser number of PV and reducing operational expenditure for operation and maintenance cost. For 1 MWp PV farm in this location annually can save to 21.45 MWh equal to 1,845 Euro and can avoid 10,467 kg of CO_2eq and 450 Euro social carbon cost and it scales up with solar farm capacity.

It is for humanity best interest that this “extra efficiency” not only be viewed as monetary and LCOE profit but also for environmental impact. The saved energy from PV solar farms can replace that comes from more potentially harmful to the environment power plants. This environmental benefit comes from reducing pollution and greenhouse gasses emission, combating climate change, lowering the social cost of carbon and many more.

For future work, a complete thermal heat transfer can provide even better accuracy thus, the model not only considers convective heat transfer but also conductive and radiative heat transfer. Implementation of the model in other racking systems will be interesting such as East – West racking system, one axis or two axis racking system where PV angles can be adjusted.

Onsite PV array testing can greatly improve this model. Because getting a complete data set of PV specification, electrical output, with corresponding meteorological data such as wind speed and wind direction are not easy to acquire. By conducting onsite testing, investors can benefit from different PV array arrangement and onsite measuring of the convection and then to be compared with the model. A deep study for utility scale PV solar farm business models can be an interesting topic as how optimizing and better model accuracy can impact the whole solar farm industry.

References

ArcGIS. (2021). *ArcGIS map viewer*. Retrieved from ArcGIS_Online: https://www.arcgis.com/index.html

Bergman, T. L. (2011). Chapter 9 - Free convection. In *Fundamentals of Heat and Mass Transfer* (p. 594). John Wiley & Sons.

Churchill, S. W. (1977). A Comprehensive Correlating Equation for Laminar, Assisting, Forced and Free Convection. *AlChE Journal (Vol. 23, No. 1)*, 10-16.

EDF. (2015). *The true cost of carbon pollution*. Retrieved from Environmental Defense Fund: https://www.edf.org/true-cost-carbon-pollution

Faiman, D. (2008). Assessing the Outdoor Operating Temperature of Photovoltaic Modules. *PROGRESS IN PHOTOVOLTAICS: RESEARCH AND APPLICATIONS - John Wiley & Sons*, 307 - 315.

Fujii, T., & Imura, H. (1972). Natural-convection heat transfer from a plate with arbitrary inclination. *Int. J. Heat Mass Transfer 15*, 755-767.

Glick, A., & Ali, N. (2020). Utility-scale solar PV performance through system-level modifcations. *Scientific Reports - Natureresearch*.

globalpetrolprices. (2021). *Singapore electricity prices, March 2021 | GlobalPetrolPrices.com*. Retrieved from GlobalPetrolPrices.com: https://www.globalpetrolprices.com/Singapore/electricity_prices/

globalsolaratlas. (2021). *Global Solar Atlas*. Retrieved from Global Solar Atlas: https://globalsolaratlas.info/map?s=-19.648165,134.189985&m=site&c=-19.648165,134.189985,11

iea. (2020). *Defining energy access: 2020 methodology – Analysis - IEA*. Retrieved from International Energy Agency: https://www.iea.org/articles/defining-energy-access-2020-methodology

iea. (2021). *Solar PV - Renewables 2020 - Analysis - IEA*. Retrieved from International Energy Agency: https://www.iea.org/reports/renewables-2020/solar-pv%20

Kaplani, E., & Kaplanis, S. (2014). Thermal modelling and experimental assessment of the dependence of PV module temperature on wind velocity and direction, module orientation and inclination. *Elsevier*, http://dx.doi.org/10.1016/j.solener.2014.05.037.

Kendoush, A. (2009). Theoretical analysis of heat and mass transfer to fluids flowing across a flat plate. *International Journal of Thermal Sciences - Elsevier*.

Libra, M., & Poulek, V. (2017). Temperature changes of I-V characteristics of photovoltaic cells as a consequence of the Fermi energy level shift. . *DOI: 10.17221/38/2015-RAE*.

McAdams, W. H. (1942). *Heat Trasmission.* New York: McGraw Hill.

Mittag, M., & Vogt, L. (2019). Thermal Modelling of Photovoltaic Modules in Operation And Production. *36th EU PV Solar Energy Conference and Exhibition.* Marseille.

NNDC. (2021). *Climate Data Online Climate Summary Help*. Retrieved from NCDC - The National Climatic Data Center - US Deppartment of Commerce: https://www7.ncdc.noaa.gov/climvis/help_wind.html

Parliament, U. (2011). *Carbon Footprint of Electricity Generation.* London: Houses of Parliament, Parliamentary Office of Science & Technology.

Sandia. (2018). *PV Performance Modeling Collaborative | Angle of Incidence*. Retrieved from sandia: https://pvpmc.sandia.gov/modeling-steps/1-weather-design-inputs/plane-of-array-poa-irradiance/calculating-poa-irradiance/angle-of-incidence/

Sandia. (2018). *PV Performance Modeling Collaborative | Plane of Array (POA) Irradiance*. Retrieved from Sandia: https://pvpmc.sandia.gov/modeling-steps/1-weather-design-inputs/plane-of-array-poa-irradiance/

Sartori, E. (2006). Convection coefficient equations for forced air flow over flat surfaces. *Sol. Energy 80*, 1063–1071.

Seia. (2021, April 30). *Utility-Scale Solar*. Retrieved from Solar Energy Industries Association: https://www.seia.org/initiatives/utility-scale-solar-power

Solcast. (2021). Retrieved from Solcast: http://www.solcast.com

Solcast. (2021). *Historical Data: Glossary of terms | Solcast - Help Center*. Retrieved from Solcast: https://articles.solcast.com.au/en/articles/2790853-historical-data-glossary-of-terms

Sparrow, E. M. (1977). Forced Convection Heat Transfer at an Inclined and Yawed Square Plate—Application to Solar Collectors. *Journal of Heat Transfer 99*.

Tuncel, B., & Akinoglu, B. G. (2018). Thermal Modeling and Verification of PV Module Temperature and Energy Yield Using Outdoor Measurements for Ankara, Turke. *IEEE*.

White, F. M. (1988). *Heat and Mass Transfer.* USA: Addison-Wesley Publishing.

WMO. (2008). *Guide to Meteorological Instruments and Methods of Observation.* Geneva: World Meteorological Organization.

World Bank. (2017). *SOLAR RESOURCE AND PHOTOVOLTAIC POTENTIAL OF INDONESIA.* World Bank.

Annex

A.1 Solar Irradiance Characteristics

These data are provided by (globalsolaratlas, 2021)

Direct normal irradiation [Wh/m^2]

	Jan	Feb	Mar	Apr	May	Jun	Jul	Aug	Sep	Oct	Nov	Dec
0 - 1												
1 - 2												
2 - 3												
3 - 4												
4 - 5												
5 - 6										7	54	37
6 - 7	217	193	121	95	73	34	32	78	231	335	373	312
7 - 8	415	445	487	556	516	478	481	560	568	567	500	446
8 - 9	515	547	599	693	664	679	700	731	702	668	601	541
9 - 10	585	630	671	777	744	768	784	814	781	749	676	606
10 - 11	630	684	731	828	800	818	832	862	835	800	724	649
11 - 12	651	700	739	838	818	845	857	888	856	800	732	652
12 - 13	635	677	717	814	799	845	861	891	855	766	692	619
13 - 14	599	648	679	779	754	821	842	871	827	722	634	582
14 - 15	542	602	628	730	712	779	806	832	774	663	583	533
15 - 16	477	566	584	661	643	707	739	770	697	594	525	473
16 - 17	398	493	497	554	513	556	603	644	567	492	430	377
17 - 18	302	380	306	223	85	88	129	244	226	231	249	271
18 - 19	51	61	6								3	37
19 - 20												
20 - 21												
21 - 22												
22 - 23												
23 - 24												
Sum	6017	6627	6763	7546	7120	7420	7666	8184	7919	7394	6775	6135

Monthly averages

Direct normal irradiation

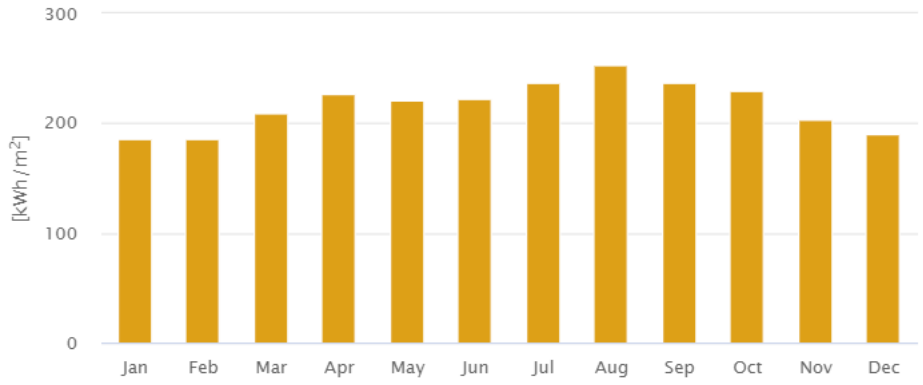

A.2 Wind Speed & direction data table

Wind Velocity	0 - 11	12 - 33	34 - 56	57 - 78	79 - 101	102 - 123	124 - 146	147 - 168	169 - 191	192 - 213	214 - 236	237 - 258	259 - 281	282 - 303	304 - 326	327 - 348	349 - 360
<0.5	3	1	2	2		2	2	1	1	1	3	4	1	2	1	1	1
0.5-1.5	19	15	16	10	14	10	11	12	14	19	10	9	14	14	20	14	8
1.5-2.5	18	43	64	98	76	50	37	10	25	10	21	12	32	26	24	31	27
2.5-3.5	50	98	153	189	232	141	108	31	11	5	11	14	36	42	33	57	34
3.5-4.5	58	137	180	209	348	441	307	43	9	2		11	17	43	50	57	56
4.5-5.5	67	117	60	88	234	517	474	36				5	13	23	26	39	31
5.5-6.5	25	57	30	68	137	460	401	8					6	17	30	11	25
6.5-7.5	9	3	5	44	46	329	410						5	28	4	9	7
7.5-8.5				6	12	198	283	2						3			
8.5-9.5						104	126	2									
9.5-10.5						18	21										
>10.5							7										

A.3 Table of air properties

Properties of air at 1 atm pressure

Temp. T, °C	Density ρ, kg/m³	Specific Heat c_p, J/kg·K	Thermal Conductivity k, W/m·K	Thermal Diffusivity α, m²/s	Dynamic Viscosity μ, kg/m·s	Kinematic Viscosity ν, m²/s	Prandtl Number Pr
−150	2.866	983	0.01171	4.158×10^{-6}	8.636×10^{-6}	3.013×10^{-6}	0.7246
−100	2.038	966	0.01582	8.036×10^{-6}	1.189×10^{-5}	5.837×10^{-6}	0.7263
−50	1.582	999	0.01979	1.252×10^{-5}	1.474×10^{-5}	9.319×10^{-6}	0.7440
−40	1.514	1002	0.02057	1.356×10^{-5}	1.527×10^{-5}	1.008×10^{-5}	0.7436
−30	1.451	1004	0.02134	1.465×10^{-5}	1.579×10^{-5}	1.087×10^{-5}	0.7425
−20	1.394	1005	0.02211	1.578×10^{-5}	1.630×10^{-5}	1.169×10^{-5}	0.7408
−10	1.341	1006	0.02288	1.696×10^{-5}	1.680×10^{-5}	1.252×10^{-5}	0.7387
0	1.292	1006	0.02364	1.818×10^{-5}	1.729×10^{-5}	1.338×10^{-5}	0.7362
5	1.269	1006	0.02401	1.880×10^{-5}	1.754×10^{-5}	1.382×10^{-5}	0.7350
10	1.246	1006	0.02439	1.944×10^{-5}	1.778×10^{-5}	1.426×10^{-5}	0.7336
15	1.225	1007	0.02476	2.009×10^{-5}	1.802×10^{-5}	1.470×10^{-5}	0.7323
20	1.204	1007	0.02514	2.074×10^{-5}	1.825×10^{-5}	1.516×10^{-5}	0.7309
25	1.184	1007	0.02551	2.141×10^{-5}	1.849×10^{-5}	1.562×10^{-5}	0.7296
30	1.164	1007	0.02588	2.208×10^{-5}	1.872×10^{-5}	1.608×10^{-5}	0.7282
35	1.145	1007	0.02625	2.277×10^{-5}	1.895×10^{-5}	1.655×10^{-5}	0.7268
40	1.127	1007	0.02662	2.346×10^{-5}	1.918×10^{-5}	1.702×10^{-5}	0.7255
45	1.109	1007	0.02699	2.416×10^{-5}	1.941×10^{-5}	1.750×10^{-5}	0.7241
50	1.092	1007	0.02735	2.487×10^{-5}	1.963×10^{-5}	1.798×10^{-5}	0.7228
60	1.059	1007	0.02808	2.632×10^{-5}	2.008×10^{-5}	1.896×10^{-5}	0.7202
70	1.028	1007	0.02881	2.780×10^{-5}	2.052×10^{-5}	1.995×10^{-5}	0.7177
80	0.9994	1008	0.02953	2.931×10^{-5}	2.096×10^{-5}	2.097×10^{-5}	0.7154
90	0.9718	1008	0.03024	3.086×10^{-5}	2.139×10^{-5}	2.201×10^{-5}	0.7132
100	0.9458	1009	0.03095	3.243×10^{-5}	2.181×10^{-5}	2.306×10^{-5}	0.7111
120	0.8977	1011	0.03235	3.565×10^{-5}	2.264×10^{-5}	2.522×10^{-5}	0.7073
140	0.8542	1013	0.03374	3.898×10^{-5}	2.345×10^{-5}	2.745×10^{-5}	0.7041
160	0.8148	1016	0.03511	4.241×10^{-5}	2.420×10^{-5}	2.975×10^{-5}	0.7014
180	0.7788	1019	0.03646	4.593×10^{-5}	2.504×10^{-5}	3.212×10^{-5}	0.6992
200	0.7459	1023	0.03779	4.954×10^{-5}	2.577×10^{-5}	3.455×10^{-5}	0.6974
250	0.6746	1033	0.04104	5.890×10^{-5}	2.760×10^{-5}	4.091×10^{-5}	0.6946
300	0.6158	1044	0.04418	6.871×10^{-5}	2.934×10^{-5}	4.765×10^{-5}	0.6935
350	0.5664	1056	0.04721	7.892×10^{-5}	3.101×10^{-5}	5.475×10^{-5}	0.6937
400	0.5243	1069	0.05015	8.951×10^{-5}	3.261×10^{-5}	6.219×10^{-5}	0.6948
450	0.4880	1081	0.05298	1.004×10^{-4}	3.415×10^{-5}	6.997×10^{-5}	0.6965
500	0.4565	1093	0.05572	1.117×10^{-4}	3.563×10^{-5}	7.806×10^{-5}	0.6986
600	0.4042	1115	0.06093	1.352×10^{-4}	3.846×10^{-5}	9.515×10^{-5}	0.7037
700	0.3627	1135	0.06581	1.598×10^{-4}	4.111×10^{-5}	1.133×10^{-4}	0.7092
800	0.3289	1153	0.07037	1.855×10^{-4}	4.362×10^{-5}	1.326×10^{-4}	0.7149
900	0.3008	1169	0.07465	2.122×10^{-4}	4.600×10^{-5}	1.529×10^{-4}	0.7206
1000	0.2772	1184	0.07868	2.398×10^{-4}	4.826×10^{-5}	1.741×10^{-4}	0.7260
1500	0.1990	1234	0.09599	3.908×10^{-4}	5.817×10^{-5}	2.922×10^{-4}	0.7478
2000	0.1553	1264	0.11113	5.664×10^{-4}	6.630×10^{-5}	4.270×10^{-4}	0.7539

A.4 JAM72S10 400 PR Specifications

JA SOLAR

MECHANICAL DIAGRAMS

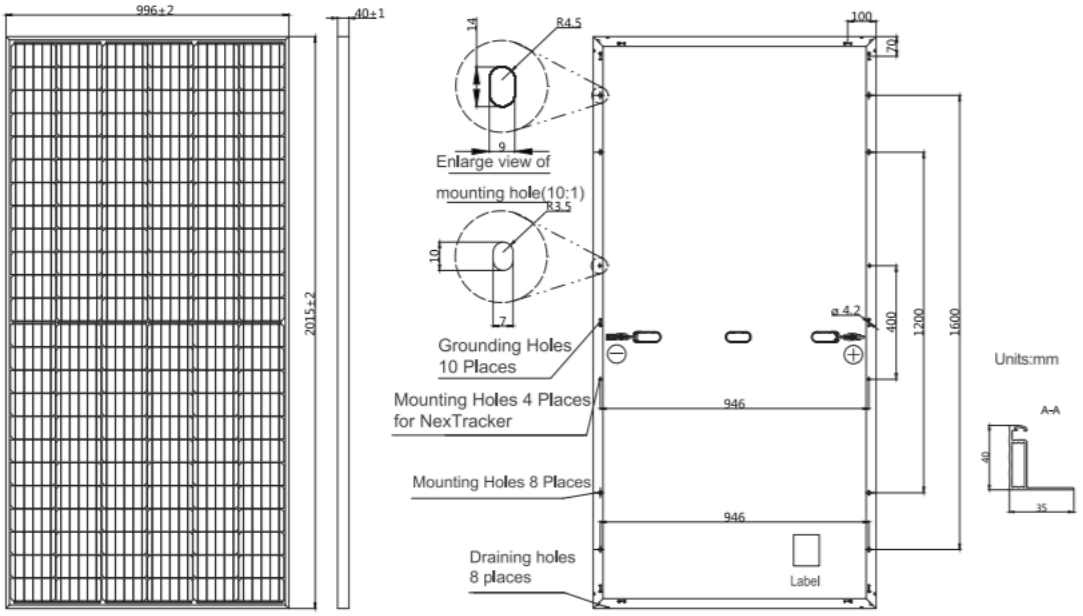

Remark: customized frame color and cable length available upon request

ELECTRICAL PARAMETERS AT STC

TYPE	JAM72S10 -390/PR	JAM72S10 -395/PR	JAM72S10 -400/PR	JAM72S10 -405/PR	JAM72S10 -410/PR
Rated Maximum Power(Pmax) [W]	390	395	400	405	410
Open Circuit Voltage(Voc) [V]	48.91	49.21	49.50	49.81	50.12
Maximum Power Voltage(Vmp) [V]	40.55	40.85	41.17	41.46	41.76
Short Circuit Current(Isc) [A]	10.16	10.21	10.26	10.32	10.37
Maximum Power Current(Imp) [A]	9.62	9.67	9.72	9.77	9.82
Module Efficiency [%]	19.4	19.7	19.9	20.2	20.4
Power Tolerance	0~+5W				
Temperature Coefficient of Isc(α_Isc)	+0.051%/°C				
Temperature Coefficient of Voc(β_Voc)	-0.289%/°C				
Temperature Coefficient of Pmax(γ_Pmp)	-0.350%/°C				
STC	Irradiance 1000W/m², cell temperature 25°C, AM1.5G				

Remark: Electrical data in this catalog do not refer to a single module and they are not part of the offer.They only serve for comparison among different module types.
*For NexTracker installations static loading performance: front load measures 2400Pa, while back load measures 2400Pa.

ELECTRICAL PARAMETERS AT NOCT

TYPE	JAM72S10 -390/PR	JAM72S10 -395/PR	JAM72S10 -400/PR	JAM72S10 -405/PR	JAM72S10 -410/PR
Rated Max Power(Pmax) [W]	289	292	296	300	303
Open Circuit Voltage(Voc) [V]	45.04	45.30	45.56	45.81	46.06
Max Power Voltage(Vmp) [V]	37.29	37.52	37.76	38.03	38.28
Short Circuit Current(Isc) [A]	8.18	8.23	8.28	8.33	8.38
Max Power Current(Imp) [A]	7.74	7.79	7.84	7.88	7.93
NOCT	Irradiance 800W/m², ambient temperature 20°C, wind speed 1m/s, AM1.5G				

OPERATING CONDITIONS

Maximum System Voltage	1000V/1500V DC(IEC)
Operating Temperature	-40°C~+85°C
Maximum Series Fuse	20A
Maximum Static Load,Front*	5400Pa
Maximum Static Load,Back*	2400Pa
NOCT	45±2°C
Safety Class	Glass Ⅱ

A.5 Helioscope annual production report

Monthly Production

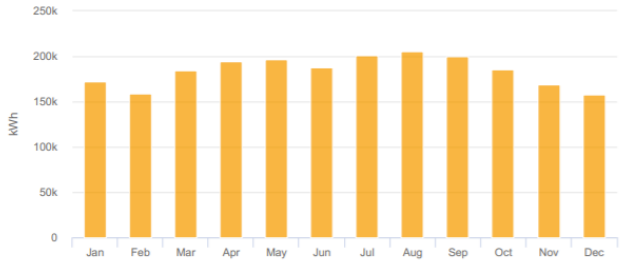

Sources of System Loss

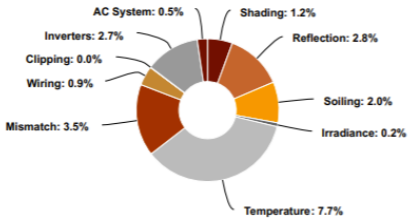

Annual Production

	Description	Output	% Delta
Irradiance (kWh/m²)	Annual Global Horizontal Irradiance	2,237.2	
	POA Irradiance	2,386.1	6.7%
	Shaded Irradiance	2,357.0	-1.2%
	Irradiance after Reflection	2,291.1	-2.8%
	Irradiance after Soiling	2,245.3	-2.0%
	Total Collector Irradiance	**2,245.3**	**0.0%**
Energy (kWh)	Nameplate	2,594,791.5	
	Output at Irradiance Levels	2,589,860.0	-0.2%
	Output at Cell Temperature Derate	2,389,797.7	-7.7%
	Output After Mismatch	2,305,649.4	-3.5%
	Optimal DC Output	2,283,767.8	-0.9%
	Constrained DC Output	2,283,385.2	0.0%
	Inverter Output	2,222,317.8	-2.7%
	Energy to Grid	**2,211,206.1**	**-0.5%**
Temperature Metrics			
	Avg. Operating Ambient Temp		28.3 °C
	Avg. Operating Cell Temp		39.9 °C
Simulation Metrics			
		Operating Hours	4622
		Solved Hours	4622